Title

Chemotherapy for pain: reversing inflammatory and neuropathic pain with the anticancer agent mithramycin A.

Journal

Pain, 165(1)

Authors

Xu, Zheyun
Lee, Man-Cheung
Sheehan, Kayla
et al.

Publication Date

2024

DOI

10.1097/j.pain.0000000000002972

Peer reviewed

Research Paper

PAIN 165 (2024) 54–74

PAIN®

OPEN

Chemotherapy for pain: reversing inflammatory and neuropathic pain with the anticancer agent mithramycin A

Zheyun Xu[a], Man-Cheung Lee[a], Kayla Sheehan[a], Keisuke Fujii[a,b], Katalin Rabl[a], Gabriella Rader[a], Scarlett Varney[a], Manohar Sharma[a], Helge Eilers[a], Kord Kober[c], Christine Miaskowski[c], Jon D. Levine[d], Mark A. Schumacher[a,*]

Abstract

The persistence of inflammatory and neuropathic pain is poorly understood. We investigated a novel therapeutic paradigm by targeting gene networks that sustain or reverse persistent pain states. Our prior observations found that Sp1-like transcription factors drive the expression of TRPV1, a pain receptor, that is blocked in vitro by mithramycin A (MTM), an inhibitor of Sp1-like factors. Here, we investigate the ability of MTM to reverse in vivo models of inflammatory and chemotherapy-induced peripheral neuropathy (CIPN) pain and explore MTM's underlying mechanisms. Mithramycin reversed inflammatory heat hyperalgesia induced by complete Freund adjuvant and cisplatin-induced heat and mechanical hypersensitivity. In addition, MTM reversed both short-term and long-term (1 month) oxaliplatin-induced mechanical and cold hypersensitivity, without the rescue of intraepidermal nerve fiber loss. Mithramycin reversed oxaliplatin-induced cold hypersensitivity and oxaliplatin-induced *TRPM8* overexpression in dorsal root ganglion (DRG). Evidence across multiple transcriptomic profiling approaches suggest that MTM reverses inflammatory and neuropathic pain through broad transcriptional and alternative splicing regulatory actions. Mithramycin-dependent changes in gene expression following oxaliplatin treatment were largely opposite to and rarely overlapped with changes in gene expression induced by oxaliplatin alone. Notably, RNAseq analysis revealed MTM rescue of oxaliplatin-induced dysregulation of mitochondrial electron transport chain genes that correlated with in vivo reversal of excess reactive oxygen species in DRG neurons. This finding suggests that the mechanism(s) driving persistent pain states such as CIPN are not fixed but are sustained by ongoing modifiable transcription-dependent processes.

Keywords: CFA, Chemotherapy, CIPN, Cisplatin, Cold pain, Cytoskeleton, Electron transport chain, HCT116, Heat pain, hyperalgesia, Intraepidermal nerve fiber, Mechanical pain, Mithramycin, Mitochondria, Nociceptor, OVCAR3, Oxaliplatin, RNAseq, Sp1, Sp4, Sex differences, Splice variant, Transcription, Transcriptome, *TRPM8*, *TRPV1*

1. Introduction

Pain associated with inflammation, traumatic nerve injury, or neurotoxicity is mediated, at least in part, by persistent activation and/or an increase in the number of ligand-gated ion channels expressed in nociceptors.[8,41] Previous studies revealed the participation of multiple genes that encode ligand-gated ion channels such as *TRPV1*: mediating inflammatory thermal (heat) hyperalgesia[15,16]; *TRPA1*: mediating inflammatory hypersensitivity[39,62]; and *TRPM8* (CMR1): mediating the sensation of cool or cold.[9,72] In response to inflammation or nerve injury, the expression of these ion channels in nociceptors change.[2,27,28,35] These findings support the hypothesis that dysregulation of nociceptor gene transcription is an important driver of persistent pain.

To understand the role of transcriptional control in nociceptors in the persistence of hypersensitive pain states, we characterized promoter regions of the *TRPV1* gene[105] and established that members of the Sp1-like transcription factor family, such as Sp4, regulate expression of *TRPV1* in sensory neurons.[20] More recently, we observed that Sp4$^{+/-}$ -knockdown mice developed acute but not persistent pain in response to both the inflammatory agent complete

Sponsorships or competing interests that may be relevant to content are disclosed at the end of this article.

Z. Xu and M.-C. Lee contributed equally.

[a] Department of Anesthesia and Perioperative Care and the UCSF Pain and Addiction Research Center, University of California, San Francisco, San Francisco, CA, United States, [b] Department of Anesthesiology, Wakayama Medical University, Wakayama, Japan, [c] Department of Physiological Nursing, School of Nursing, University of California, San Francisco, CA, United States, [d] Division of Neuroscience, Departments of Medicine and Oral and Maxillofacial Surgery, University of California San Francisco, San Francisco, CA, United States

**Corresponding author. Address: Department of Anesthesia and Perioperative Care and the UCSF Pain and Addiction Research Center, University of California, San Francisco, San Francisco, CA 94143, United States. Tel.: +1 4155027022. E-mail address: Mark.Schumacher@ucsf.edu (M. A. Schumacher).*

Supplemental digital content is available for this article. Direct URL citations appear in the printed text and are provided in the HTML and PDF versions of this article on the journal's Web site (www.painjournalonline.com).

http://dx.doi.org/10.1097/j.pain.0000000000002972

Freund adjuvant (CFA) and nerve growth factor (NGF), as well as to the platinum-based chemotherapy agent oxaliplatin.[90] In addition to *TRPV1*, Sp4 regulated other genes (*TRPA1* and *TRPM8*) critical for pain persistence.[90] Taken together, these findings stimulated our interest in the transcriptional inhibitor mithramycin A (MTM), a chemotherapeutic agent that blocks members of the Sp1-like transcription factor family.[96]

Mithramycin (Plicamycin) blockade of Sp1-like factors is foundational to its action as treatment for embryonal and testicular cancers,[13,96] and cancer-related hypercalcemia and Paget disease. Although several clinical studies reported MTM-associated improvements in pain,[21,43] these findings may be related to a decrease or reversal of the underlying disease. Nevertheless, in one clinical series, 10 of 15 patients with widespread osseous metastases from breast cancer achieved rapid pain relief following MTM treatment despite continued advancement of boney metastases and no evidence of bone healing.[25]

Previously, we observed that MTM dose-dependently inhibited *TRPV1* transcription, in vitro[20] and *TRPV1* expression (mRNA, protein, activity) in cultured dorsal root ganglion (DRG) neurons.[108] In this study, we investigated whether the actions of MTM observed in vitro, extend to reversal of inflammatory heat hyperalgesia (a *TRPV1*-mediated process) and extend to painful chemotherapy-induced peripheral neuropathy (CIPN)[75,79] induced by cisplatin and oxaliplatin.[49,99] Administration of MTM to mice reversed behavioral models of painful heat/mechanical/cold hypersensitivity induced by inflammation and platinum-based chemotherapy. Mechanisms underlying MTM's reversal of hypersensitivity were investigated.

2. Methods

2.1. Animals

C57Bl/6 male and female mice (8-12 weeks) were obtained from the Jackson Laboratory (Bar Harbor, ME) or bred and housed within the UCSF animal care facility in a climate-controlled room on a 12-hours light/dark cycle. Laboratory diet was available ad libitum, except when the mice were being tested.

2.2. Drug administration

2.2.1. Intraplantar injections

Complete Freund adjuvant (Sigma-Aldrich, St. Louis, MO)[86] 20-μL emulsified with saline or saline vehicle alone was injected into the plantar surface of the left hindpaw under isoflurane anesthesia.

2.2.2. Intraperitoneal injections

Cisplatin, oxaliplatin (Sigma-Aldrich), or vehicle (saline) was injected intraperitoneally (i.p.) (3 mg/kg).[49] Mithramycin A (MTM) (Enzo Life Sciences, Farmingdale, NY) or vehicle (1% DMSO in saline) was injected ip (10-100 μg/kg).

2.3. Behavioral assessments

Efforts were made to minimize the number of mice used and their discomfort. Experimental protocols were approved by the University of California, San Francisco, Institutional Animal Care and Use Committee (IACUC) and adhered to the NIH Guidelines for the Care and Use of Laboratory Animals. Investigators who conducted behavioral tests were blinded to treatment condition, and animals were randomized to groups.

2.3.1. Heat paw withdrawal

Hargreaves test (thermal heat) was performed on mice that were acclimated, and baseline measurements were taken on day −1 and 0 before injection. Heat sensitivity was based on using an infrared heat source aimed at the plantar surface of the left hindpaw and measuring the paw withdrawal latency in seconds.[42] Measurements were taken 3 times per testing point with a maximum cutoff time of 20 seconds and with at least 5 minutes of rest between the tests.

2.3.2. Mechanical paw withdrawal threshold

von Frey test (mechanical): Mechanical sensitivity was quantified as a paw flinch and/or withdrawal response to calibrated von Frey monofilaments using the "up–down" method.[17] This procedure was applied 4 times following the first change in response and completed 3 times per mouse, with at least 10 minutes of rest between each test.

2.3.3. Antagonist to TRPA1-activated paw licking and TRPM8-activated wet dog shakes

Mice were treated with either *TRPA1* antagonist HC-030031 (APE xBIO, 100 mg/kg, ip) or 0.5% methylcellulose as vehicle, 2 hours before the administration of *TRPA1* agonist allyl isothiocyanate (AITC) (20 μL of 0.1% in saline, i.pl.) under isoflurane anesthesia. After 5 to 10 minutes of recovery from anesthesia, mice were observed for AITC-elicited paw licking behaviors for 20 minutes in plexiglass enclosures.

TRPM8 agonist icilin (20 mg/kg in 20% DMSO/80% phosphate-buffered saline [PBS], i.p.) elicits pronounced wet dog shakes in rodents. Two hours after pretreatment of *TRPM8* antagonist AMG333 (Tocris, 3 mg/kg, orally) or 2% methylcellulose/1% Tween-80, pH 9.0 as vehicle, mice injected with icilin were immediately observed, and the number of wet dog shakes were counted for 30 minutes in plexiglass enclosures.

2.3.4. Cold plate paw withdrawal

Following acclimation, mice were tested at 10°C and following a 20-minutes rest interval, again at 4°C, for a maximal observation period of 20 second/trial using a Cold Plate (Bioseb, Pinellas, FL) and translucent chamber. The time (seconds) until the first paw flinch/shake/licking was recorded, and trials were performed in triplicate.[90]

2.4. Cell culture

Primary DRG neurons were cultured from 8- to 12-week-old adult male or female mice (C57Bl/6) using methods previously described.[85,108] HCT116 cells (ATCC) were maintained in McCoy 5a media supplemented with 10% fetal bovine serum (Corning, Tewksbury, MA) and 1% penicillin-streptomycin. OVCAR3 cells (ATCC) were maintained in ATCC-formulated RPMI-1640 medium (Gibco-Thermo Fisher, Waltham, MA) supplemented with 20% fetal bovine serum (Corning), 0.01 mg/mL bovine insulin (Sigma-Aldrich), and 1% penicillin–streptomycin.

2.5. Calcium imaging and microscopy

Measurement of $[Ca^{2+}]_i$ and cell size determinations in primary DRG neurons were performed by preloading cultured neurons plated on coverslips with 5-μM cell permeant Fluo-4 AM

(Invitrogen) calcium-sensitive dye (488/520 nm) with Pluronic F-127 (Invitrogen, Waltham, MA) for 45 to 50 minutes at 37°C, 5% CO_2. Dorsal root ganglion neurons were visualized through a Zeiss Axiovert microscope (10x) equipped with an Axiocam camera and quantified using Zen Pro software (Carl Zeiss, Jena, Germany). Dorsal root ganglion neurons were perfused with Hank buffered salt solution with calcium and magnesium, supplemented with 20 mM HEPES and 1% penicillin–streptomycin, at 2 mL/minute at room temperature (22°C) before cold buffer or KCl (50 mM) stimulation. Cold perfusion buffer was applied for 30 seconds with a final bath temperature of 11.3°C (range, 10.5-12.1°C) at the end of cold buffer application, using a cold perfusion unit (TC-RD Bioscience Tools, San Diego, CA). Neurons that responded within 15 seconds after cold buffer application by an increase of $[Ca^{2+}]_i \geq$ 20% from baseline values were defined as responders. Neurons that did not respond to KCl were excluded.

2.6. qRT-PCR

Quantitative Reverse Transcription PCR RNA was isolated from mouse lumbar DRG (Trizol Reagent, Invitrogen), and first strand complementary DNA was prepared (SuperScript III First-Strand Synthesis System, Invitrogen-Thermo Fisher, Waltham, MA). Using the QuantiStudioTM 6 Flex Real-Time PCR system (Applied Biosystems, Waltham, MA), mRNA expression levels were quantified using iTaq Universal SYBR Green Supermix assays (Bio-Rad, Hercules, CA) for TRPM8 (F:GTGTCTTCTTTACCAGA-GACTCCAAGGCCA;R:TGCCAATGGCCACGATGTTCTCTTCT-GAGT), normalized by GAPDH (F: TGCGACTTCAACAGCAACTC; R: CTTGCTCAGTGTCCTTGCTG) expression, and represented as relative quantitation (RQ) using the comparative $\Delta\Delta C_T$ method.[20,88,90,108]

2.7. Immunohistochemistry: intraepidermal nerve fiber

The glabrous skin of the mouse footpad (hind paws) was removed and fixated in 4% PFA at 4°C overnight. Samples were transferred to 20% (wt/vol) sucrose for at least 24 hours and embedded in optimal cutting temperature (OCT) compound, frozen, and sliced into 25-μm sections using a cryostat. Sections were washed in PBS and incubated at room temperature (RT) for 2 hours in blocking solution (5% normal donkey serum [NDS] and 0.3% Triton X-100 in PBS). Free-floating sections were incubated with primary antibody PGP9.5 (panneuronal marker) (rabbit anti-mouse polyclonal, 1:200 dilution, Thermo-Fisher) in wash buffer (1% NDS and 0.3% Triton X-100 in PBS) at RT for 2 hours. Following 3 washes in wash buffer, slices were incubated overnight at 4°C with a 1:400 dilution of donkey anti-rabbit Cy3 secondary antibody (Millipore Burlington, MA) in wash buffer solution. Sections were washed 3 times in PBS, mounted onto slides (Aqua-Polymount, Thermo-Fisher), and imaged using Keyence microscope and software (Keyence Corp. of America, Pleasant Hill, CA). Five sections from each mouse were randomly chosen for intraepidermal nerve fiber (IENF) quantification and 3 fields of view per section using a ×40 objective. The length of the epidermis within each field of view was measured using ImageJ software, and the density of fibers was determined as number of nerve fibers per millimeter. The experimenter was blinded to experimental conditions.

2.8. Apoptosis

OVCAR3 and HCT116 cells (~ 5000 cells/per well) in a 96-well format (Falcon, Corning Tewksbury, MA) were cultured overnight. Following 24 hours of treatment, apoptosis activity was measured using Caspase Glo 3/7 Assay System (Promega, San Luis Obispo, CA) following manufacturer's protocol. Luminescence was recorded by Cytation 5 Cell Imaging Multi-Mode Reader (BioTek, Winooski, VT) in triplicate measures.

2.9. Measurement of reactive oxygen species in dorsal root ganglion neurons

Adult male mice (8-12 week old) were treated in vivo with oxaliplatin (3 mg/kg, i.p.) at day 0, followed by MTM (100 μg/kg, i.p.) 48 hours and 72 hours postinjection. On day 10, mice were euthanized under carbon dioxide, and approximately half of the total DRGs were harvested and cultured with the addition of uridine to a final concentration of 20 μM. CellROX (5 μM) Green Reagent (Invitrogen-Thermo Fisher) was added to the cells for 30 minutes following manufacturer's protocol. Then, 100-μL Live-Cell Imaging Solution (Invitrogen-Thermo Fisher) was added. Imaging and analysis were performed on Cytation5 using Gen5 software (BioTek, Agilent, Santa Clara, CA).

2.10. Statistical analysis

Nociceptive thresholds were expressed as means ± SEM. When applicable, detection of behavioral differences between multiple groups was performed by 2-way repeat-measures analysis of variance (RM-ANOVA) or 1-way ANOVA followed by Tukey post hoc test. When indicated, independent-sample *t*-tests and Fisher exact tests were done. A P value of <0.05 was considered statistically significant. Analysis was performed using Prism (GraphPad Software). Figures were composed using Adobe Illustrator and BioRender.

2.11. Transcriptomics

2.11.1. RNA sample preparation/data curation

Lumbar DRG were dissected from euthanized mice (n = 5 for each treatment group). Total DRG RNA was extracted from mice treated with oxaliplatin + vehicle (OV), oxaliplatin + MTM rescue (OM), vehicle + vehicle (VV), and vehicle + MTM (VM) using TRIzol reagent (Invitrogen). Quality was assessed using the Agilent Bioanalyzer device. Total RNA was treated with the Illumina Globin-Zero Gold rRNA removal kit (Illumina, San Diego, CA). Complementary DNA libraries were constructed with the Illumina Truseq kit. Sequencing of the 20 samples was performed at the UC Davis Genomics Core Facility on the NovaSeq 6000 system (Illumina) with the goal of 50 million paired end reads or greater. RNAseq data processing was performed based on best practices[22,56] and our previous experience.[52] Individual samples were inspected with FASTQC and in aggregate with MultiQC.[30] Reads were aligned to the GRCm38 assembly (GENCODE vM23). Gene expression levels were summarized at the gene level using featureCounts.[64] Replicate count data were processed in edgeR.[87] Ensembl[109] transcripts were annotated with Entrez gene ID and symbol.[69] Lowly expressed tags were filtered to retain those with 1 read per million or greater. Count estimates were normalized with the trimmed means of M values (TMM) method.[87] Then, TMM normalization was applied to the data set in edgeR using calcNormFactors. Surrogate variable analysis was used to identify variations that contributed to heterogeneity in the sample (eg, batch effects) that were not due to the variable of interest (eg, oxaliplatin treatment).[60] Any surrogate variable that was significantly associated with the phenotype was excluded. All

other surrogate variables were included as covariates in the differential expression final regression model.

2.11.2. Differential gene expression analysis

Differential expression was determined under a variance modeling strategy that addressed the overdispersion observed in gene expression (GE) count data.[59] We assessed the significance of the transcriptome-wide analysis to identify differentially expressed genes (DEGs) using a strict false discovery rate (FDR) of <0.05 under the Benjamini–Hochberg (BH) procedure and no minimal fold-change as evaluated by the topTags and p.adjust R functions.[44]

Pathway analysis was performed using the Metascape tool. Differentially expressed genes were searched against published sources of annotated pain gene databases.[53,58,73] In addition, the gene identifiers were searched in PubMed in automated fashion using the easyPubMed package in R. Pertinent hits were manually curated for relevance.

2.11.3. Differential splice analysis

Following our previously published methodology,[33] differential splice analysis was performed. Analysis of differential alternative RNA splicing was performed using the replicate multivariate analysis of transcript splicing (rMATS) tool.[91] We assessed significance of the differential alternative splicing with an FDR cutoff of <0.001. For each splicing event, a ratio was calculated for each sample between transcripts found to include that splicing event and those found specifically without that splicing event. Unsupervised principal component analysis was performed on the samples' splice junction inclusion ratios within R.

3. Results

3.1. Mithramycin reverses inflammatory heat hyperalgesia

We previously demonstrated that binding of Sp4 or Sp1 to the *TRPV1* promoter P2 region drives the expression of *TRPV1* mRNA in cultured mouse DRG neurons.[20] Mithramycin, a Sp1-family transcription inhibitor, was shown to block *TRPV1* expression in nociceptors.[108] Therefore, we examined if systemic treatment of mice with MTM would block ongoing inflammatory heat hyperalgesia, a *TRPV1*-dependent pain behavior.[15,16] Following induction of peripheral inflammation by intraplantar (i.pl) injections of CFA, we observed a decrease in paw withdrawal latency (heat hyperalgesia) from a baseline value of 11.6 ± 0.6 to 6.3 ± 0.3 seconds at 48 hours. After 2 sequential daily injection of MTM (100 μg/kg i.p), a dose based on its anticancer and neuroprotective activity in mice,[32] a time-dependent reversal of heat hyperalgesia was observed (**Fig. 1A**), with heat thresholds approaching baseline values at day 6 (11.4 ± 0.6 seconds $P = 0.028$) and day 10 (11.6 ± 0.6 seconds $P = 0.0025$), as compared with the vehicle-treated CFA mice with a mean latency of 8.7 ± 0.4 seconds on day 10. Mithramycin did not change heat thresholds when given alone. Importantly, MTM-induced reversal of inflammatory heat hyperalgesia occurred without a measurable change in the development of CFA-induced paw thickness (edema) (**Fig. 1B**).

To determine if MTM-induced reversal of hyperalgesia in male mice was observed in female mice, we evaluated the ability of CFA to induce heat hyperalgesia in female mice compared with male mice. As shown in (**Fig. 1C**), male and female mice had indistinguishable baseline thermal paw withdrawal latencies. Female mice developed a greater decrease in paw withdrawal latency (heat hyperalgesia) at days 1 ($P = 0.001$), 6 ($P < 0.0001$), and 10 ($P = 0.001$), as compared with male mice. After 2 sequential daily injections of MTM beginning at 48 hours, a time-dependent reversal of heat hyperalgesia was observed in both male and female mice (**Fig. 1D**). However, female mice showed a less robust MTM reversal of heat hyperalgesia with MTM reversal latencies at days 6 ($P = 0.007$) and 10 ($P = 0.0001$), attaining values equivalent to untreated CFA-male mice (inflammatory heat hyperalgesia). By contrast, MTM treatment reversed CFA-treated male mice to baseline latency values on days 6 ($P = 0.007$) and 10 ($P = 0.0004$).

3.2. Mithramycin reverses cisplatin-induced heat and mechanical hypersensitivity

Cisplatin is associated with dose-limiting side effects primarily due to its neurotoxic effects on sensory neurons.[38,71] Behavioral models of cisplatin-induced hypersensitive states induce both heat and mechanical hypersensitivity.[99] As shown in (**Fig. 1E**), cisplatin treatment was associated with a reduction in heat paw withdrawal latency, from baseline values of 15.0 ± 1.2 to 9.6 ± 1.2 seconds at 48 hours. Following 2 daily treatments of MTM, heat withdrawal latencies returned to baseline values of 14.8 ± 1.2 seconds on day 4 and stayed near baseline values through day 14 (14.7 ± 0.9 seconds $P = 0.0009$). By comparison, vehicle-treated cisplatin mice maintained a reduced heat latency of 10.1 ± 0.5 seconds on day 14. To determine if MTM was able to reverse other modalities of cisplatin-induced hypersensitivity, changes in mechanical threshold were measured. Cisplatin, administered daily for 5 days, induced a reduction in mechanical threshold values from a baseline of 0.91 ± 0.03 g to 0.18 ± 0.03 g on day 2. Following MTM treatment (**Fig. 1F**), mechanical thresholds reversed towards baseline, attaining near baseline values of 0.83 ± 0.09 g on day 7 that were sustained through day 21 ($P < 0.0001$).

3.3. Mithramycin reverses oxaliplatin-induced cold and mechanical hypersensitivity

Chemotherapy-induced peripheral neuropathy pain is a dose-limiting side effect induced by oxaliplatin.[55] Given our previous observations that oxaliplatin-induced cold and mechanical hypersensitivity were reversed in $Sp4^{+/-}$-knockdown mice,[90] we investigated whether the use of MTM would result in a similar reversal. Using doses of MTM tested in models of cancer (Ewing sarcoma)[40] and neurodegeneration (Huntington disease [HD])[32] and the lowest profile of toxicity, we compared a single dose of MTM at 10, 50, or 100 μg/kg to reverse oxaliplatin (3 mg/kg)-induced cold (10°C) hypersensitivity. As shown in **Fig. 2A**, oxaliplatin (3 mg/kg i.p.) induced a decrease in paw withdrawal latency (cold hypersensitivity) at 48 hours ($P = 0.0008$) and 72 hours ($P < 0.0001$). Reversal of cold hypersensitivity was achieved at 72 hours following MTM at 100 μg/kg ($P = 0.0024$) but not at 10 or 50 μg/kg. Overall, MTM appears to reverse behavioral models of nociceptive pain at a 10-fold lower dose than required to reduce an experimental tumor model and within the working dose range to increase survival in a model of HD.[32,40] Then, we studied the persistence of oxaliplatin-induced cold hypersensitivity following MTM treatment (**Fig. 2B**). Oxaliplatin-induced a decrease in 10°C paw withdrawal latency in male mice from 15.9 ± 1.0 to 10.7 ± 0.7 seconds at 24 hours. Mithramycin treatment resulted in a reversal of oxaliplatin-induced hypersensitivity, achieving baseline values of

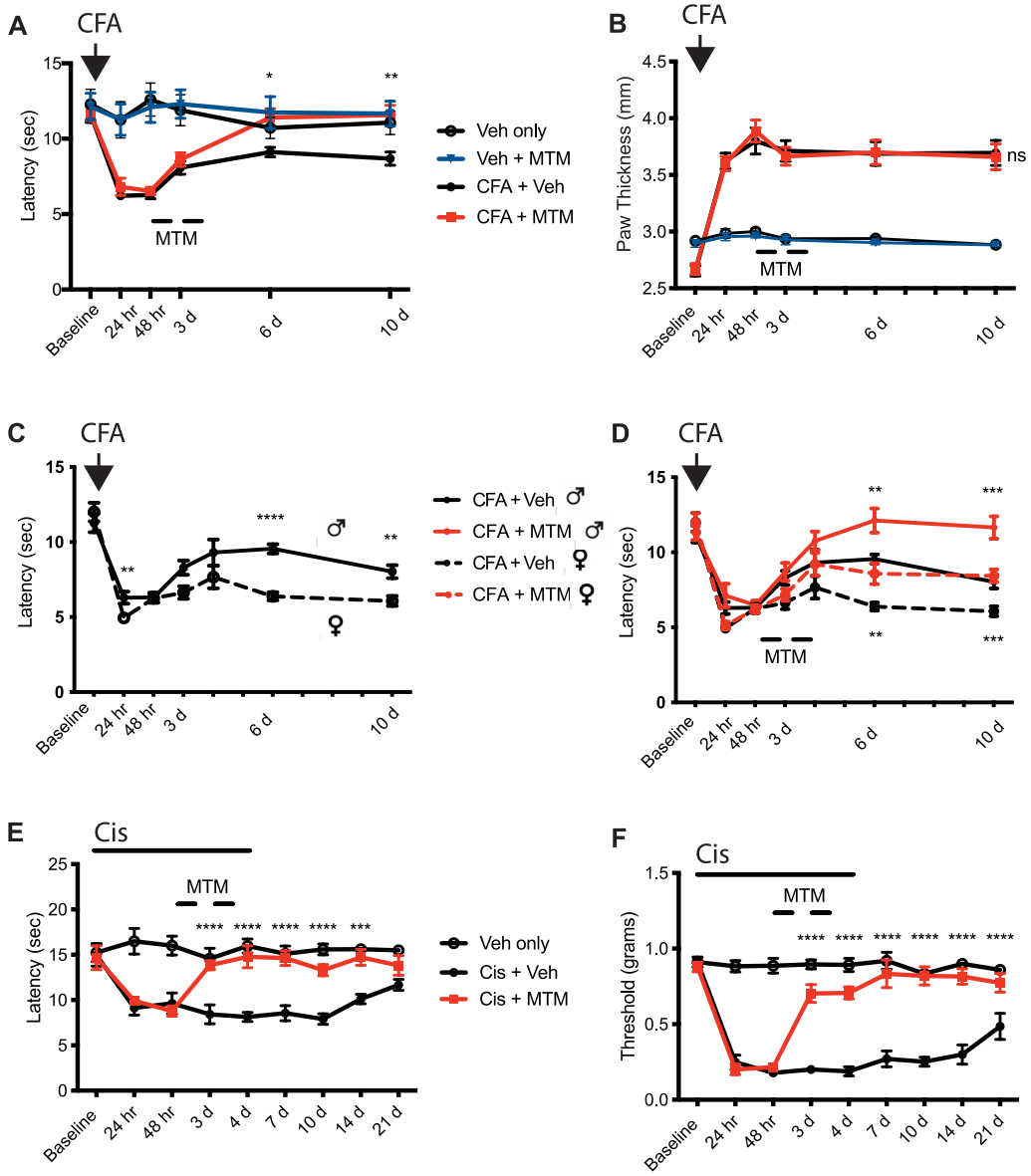

Figure 1. MTM reverses CFA- and cisplatin-induced thermal (heat) hyperalgesia. (A) Hindpaw injection of CFA induced inflammatory heat hyperalgesia (decrease in thermal paw withdrawal latency) at 24 and 48 hours and was reversed to baseline control values in male mice after MTM treatment (100 μg/kg ip,—bars) on day 6 (*$P = 0.028$) and day 10 (**$P = 0.0025$); n = 17. MTM did not change heat thresholds when given alone, n = 10. (B) An increase in CFA-induced hindpaw thickness (inflammation) was unchanged by MTM treatment (ns = not significant). (C) Comparison of CFA-induced inflammatory heat hyperalgesia between female and male mice. Despite equivalent baseline latencies, female mice developed a greater CFA-induced decrease in latency (heat hyperalgesia) compared with male mice on days 1 (**$P = 0.001$), 6 (****$P < 0.0001$), and 10 (**$P = 0.001$); multiple *t* tests; n = 11. (D) MTM directed reversal of heat hyperalgesia in CFA-treated female mice on days 6 (**$P = 0.007$) and 10 (***$P = 0.0001$); multiple t tests; n = 14 but was less than that found in MTM-treated male mice on days 6 (**$P = 0.007$) and 10 (***$P = 0.0004$); multiple *t* tests; n = 11. MTM-treated female mice attained latency values observed for untreated CFA-male mice on days 6 and 10, whereas MTM-treated male mice recovered to baseline values on the same time points. (E) Cisplatin (Cis) (3 mg/kg ip) administered daily for 5 days decreased heat paw withdrawal latency at 24 hours. Paw withdrawal latency was reversed to baseline values following MTM treatment starting on day 3 through day 14 (****$P < 0.0001$; ***$P = 0.0009$); n = 6. (F) Cisplatin treatment (5 days)-induced mechanical hypersensitivity (decrease in mechanical threshold) beginning at 24 hours was reversed following MTM treatment to baseline values by day 7 through day 21 (****$P < 0.0001$); n = 6. Statistical comparison: 2-way RM ANOVA with Tukey post hoc test. Mean values ± SEM. CFA, complete Freund adjuvant; MTM, mithramycin; RM ANOVA, repeated-measures analysis of variance; Veh, vehicle.

16.4 ± 0.9 seconds from day 3 to day 14 ($P < 0.0001$), through day 21 ($P = 0.022$). When testing was repeated at 4°C (**Fig. 2C**), MTM demonstrated a similar reversal on days 3 ($P = 0.0083$), 6 ($P < 0.0001$), 10 ($P = 0.0016$), 14 ($P = 0.016$), and 21 ($P < 0.0001$). Mithramycin alone (**Figs. 2B and C**) failed to change baseline paw withdrawal latency in control mice.

Mechanical hypersensitivity associated with oxaliplatin treatment has been modeled in rodents.[48,74,75,94] As shown in **Fig. 2D**, oxaliplatin induced a robust decrease in mechanical nociceptive threshold from a baseline of 0.85 ± 0.01 g to 0.20 ± 0.02 g at 48 hours after oxaliplatin treatment. Mithramycin produced marked reversal of mechanical hypersensitivity to baseline values of 0.83 ± 0.05 g by days 3 to 10 ($P < 0.0001$) that began to diminish on day 14 ($P = 0.044$). Mithramycin did not change mechanical thresholds when given alone.

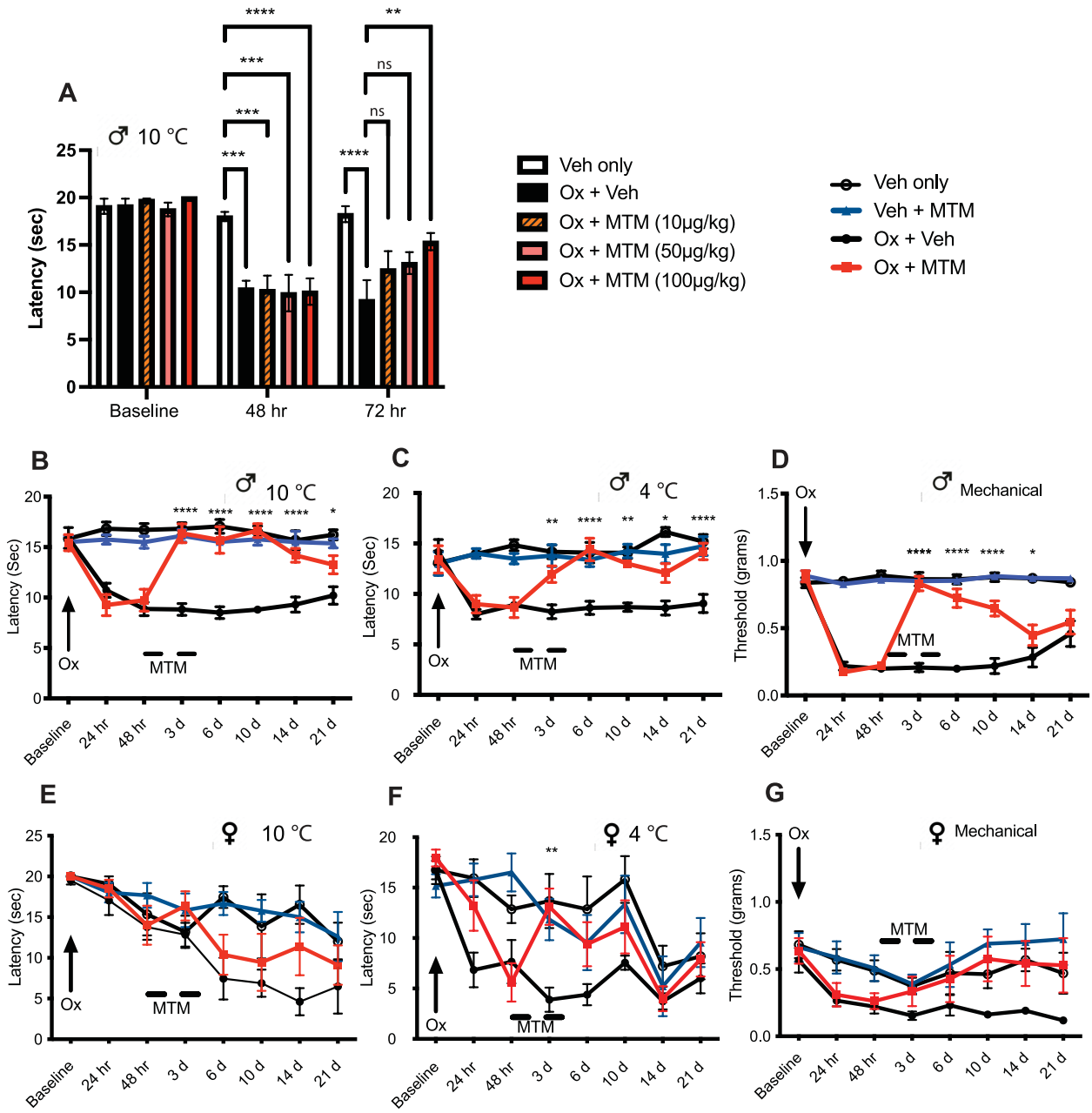

Figure 2. MTM reverses oxaliplatin-induced cold and mechanical hypersensitivity. (A) Oxaliplatin (OX) (3 mg/kg ip) induced a decrease in paw withdrawal latency (cold hypersensitivity) at 48 hours (***$P = 0.0005$) and 72 hours (****$P < 0.0001$). Reversal of cold hypersensitivity was achieved at 72 hours following MTM treatment 10 μg/kg, 50 μg/kg, and more so at 100 μg/kg (*$P < 0.05$, ns = not significant); n = 4. (B) Longitudinal study of MTM (100 μg/kg ip,—bars) reversed the oxaliplatin-induced cold hypersensitivity on days 3, 6, 10, 14, and 21 (*$P = 0.022$, ****$P < 0.0001$); n = 6. Control oxaliplatin-treated mice maintained cold hypersensitivity through day 21. MTM alone did not change paw withdrawal latency to 10°C. (C) Testing was repeated at 4°C demonstrating reversal on days 3 (**$P = 0.0083$), 6 (****$P < 0.0001$), 10 (**$P = 0.0016$), 14 (*$P = 0.016$), and 21 (****$P < 0.0001$); n = 6. (D) Oxaliplatin treatment induced a decreased mechanical threshold (mechanical hypersensitivity) at 24 and 48 hours that was reversed on days 3, 6, 10, and 14 following MTM treatment (bar) (*$P = 0.044$, ****$P < 0.0001$); n = 6. MTM did not change mechanical thresholds when given alone. (E to G) Oxaliplatin-treated female mice following MTM-rescue showed limited ability to reverse cold (4°C) hypersensitivity on days 3 (**$P = 0.0052$) or mechanical hypersensitivity on day 10 ($P = 0.051$) and day 21 ($P = 0.053$); n = 6. Statistical comparison: 2-way RM ANOVA with Tukey *post hoc* test. Mean values ± SEM. MTM, mithramycin; RM ANOVA, repeated-measures analysis of variance; Veh, vehicle.

To determine if MTM pretreatment could prevent oxaliplatin-induced mechanical hypersensitivity, MTM was administered on day −1 and again 45 minutes before oxaliplatin administration on day 0. As shown in (Supplementary Figure 1, available at http://links.lww.com/PAIN/B865), pretreatment with MTM reduced the magnitude of mechanical hypersensitivity on days 1 to 3 as compared with oxaliplatin-only control at 24 hours, 48 hours, and day 3 ($P < 0.0001$).

Given our finding that MTM reversed CFA-induced inflammatory heat hyperalgesia to a greater degree in male than female mice (**Fig. 1D**), we evaluated the ability of MTM to reverse oxaliplatin-induced cold and mechanical hyperalgesia in female mice. As shown in **Figs. 2E, F, G**, although oxaliplatin induced equivalent hypersensitivity in male and female mice, oxaliplatin-treated female mice showed trends of MTM reversal of cold and mechanical hypersensitivity,

reaching significance on day 3 at 4°C ($P = 0.0052$). To quantitate differences in MTM rescue between male and female mice, we examined the percent efficacy of MTM reversal of CFA and oxaliplatin-induced hypersensitivity. As shown in Supplementary Figure 2, available at http://links.lww.com/PAIN/B865, MTM was approximately 50% more efficacious in male mice reversing inflammatory heat hyperalgesia on all days measured: day 3 ($P = 0.021$), day 4 ($P = 0.014$), day 6 ($P = 0.0013$), and day 10 ($P = 0.017$). Mithramycin was more efficacious in male mice at reversing oxaliplatin-induced cold (10°C) hypersensitivity on day 6 ($P = 0.010$) and day 10 ($P = 0.034$).

3.4. Mithramycin reverses oxaliplatin-induced cold responsiveness of dorsal root ganglion neurons

Platinum-based chemotherapy primarily drives neurotoxicity through their transport and accumulation in peripheral sensory neurons.[38,55,71,74] Platinum agents, such as oxaliplatin, are largely, but not completely, excluded from the CNS.[46] Therefore, painful cold and mechanical hypersensitivities arising from oxaliplatin may be driven by alterations in peripheral sensory neurons. To test our hypothesis that the target for systemically administered MTM to reverse hypersensitivity to cold resides, at least in part, in the sensory neurons, we measured changes in the percentage of DRG neurons (ex vivo) that were activated by the application of cold buffer following

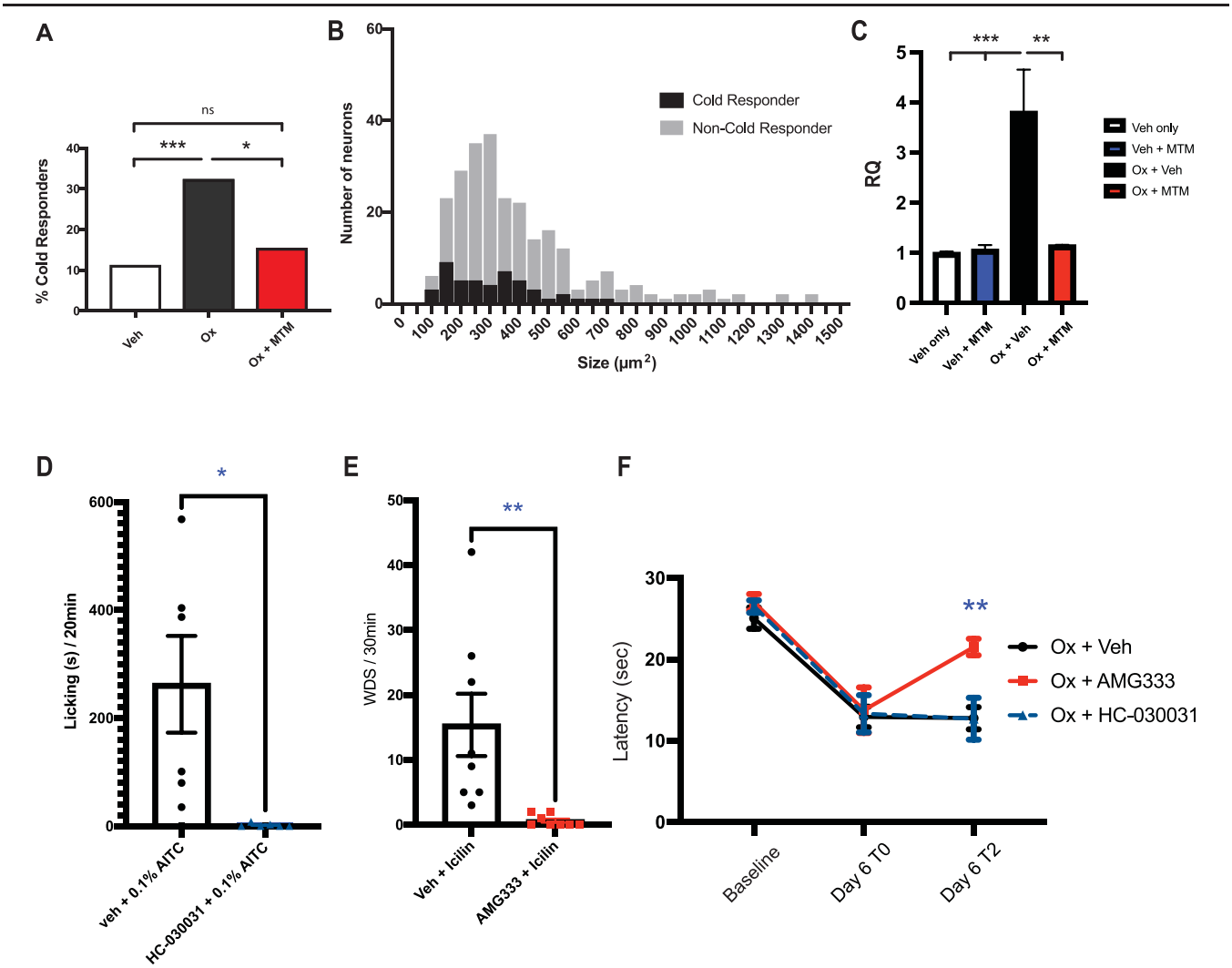

Figure 3. MTM reversal of oxaliplatin-induced cold hypersensitivity is linked to *TRPM8* expression in DRG neurons. (A) Percentage of DRG neurons responding to cold buffer (10.5-12.1°C; mean 11.3°C) derived from mice treated in vivo with vehicle (Veh), oxaliplatin (OX) (3 mg/kg), or OX + MTM (100 μg/kg) as conducted in Figure 2B and harvested on day 4. MTM reversed the increased number of cold-responding DRG neurons ex vivo. n = 3 independent trials, total neurons = 257 (Fisher exact test $^{*}P = 0.019$, $^{***}P = 0.0008$, ns = not significant). (B) Size distribution histogram of cold responding DRG neurons (black, n = 47) were of smaller size than nonresponders (grey, n = 210) ($P < 0.0001$ unpaired *t* test, Welch correction). (C) DRG TRPM8 mRNA expression (RQ) was increased approximately 4 fold following oxaliplatin treatment in vivo. MTM (100 μg/kg) reversed the OX-induced increase in DRG TRPM8 mRNA expression to baseline levels (1-way ANOVA with Tukey post hoc test ($^{**}P = 0.001$; $^{***}P = 0.0006$); n = 5, triplicate measures. mean ± SEM. (D) Validation of TRPA1 antagonist HC-030031 to block AITC-induced paw licking. Mice received HC-030031 (100 mg/kg i.p.) at 2 hours. Postantagonist, 0.1% AITC (20 μL, ipl, in saline), was administered. AITC-elicited licking behaviors(s) were completely blocked by HC-030031 ($^{*}P = 0.015$); n = 6. Unpaired *t* test. (E) Validation of TRPM8 antagonist AMG333 to block icilin-induced wet dog shakes (WDS). Mice administered AMG333 (3 mg/kg, p.o), and 2 hours later, icilin (20 mg/kg ip) completely blocked icilin-induced WDS ($^{**}P = 0.0085$); n = 8. Unpaired *t* test. (F) Mice were treated with OX on day 0 and developed cold hypersensitivity (decreased withdrawal latency to 10°C) on day 6, T0, TRPM8 antagonist AMG333 reversed the cold hypersensitivity 2 hours post the administration on day 6, T2 ($^{**}P = 0.002$) n = 7 to 9. Statistical comparison: 2-way ANOVA. Mean ± SEM. Administration of TRPA1 antagonist HC-030031 failed to reverse OX-induced cold hypersensitivity. AITC, allyl isothiocyanate; ANOVA, analysis of variance; DRG, dorsal root ganglion; MTM, mithramycin.

in vivo treatments with oxaliplatin with or without MTM. As shown in **Fig. 3A**, the percentage of cold responsive primary DRG neurons was higher in oxaliplatin-treated mice compared with vehicle controls ($P = 0.0008$). By contrast, DRG neurons derived from mice receiving oxaliplatin plus MTM showed a reduced percentage of cold activated neurons ($P = 0.019$). In addition, cold responsive DRG neurons had a smaller size distribution (**Fig. 3B**), with a mean area of 304 ± 22 μm^2 compared with cold nonresponders 423 ± 19 μm^2 ($P < 0.0001$). These findings support our hypothesis that MTM in vivo reverses oxaliplatin-induced hypersensitivity to a cold stimulus, in part, through its action on small-diameter sensory neurons.

3.5. Mithramycin inhibition of oxaliplatin cold hypersensitivity is associated with reversal of TRPM8 *overexpression in dorsal root ganglion neurons*

TRPM8, a channel activated by cold temperatures (26°C-15°C), expressed in a subset of small-diameter DRG neurons,[9,51,72] is proposed to be a transducer of painful oxaliplatin-induced cold hypersensitivity.[35] We investigated whether the MTM reversal of oxaliplatin-induced cold hypersensitivity was linked to changes in *TRPM8* expression in DRG. We confirmed oxaliplatin's ability to induce cold hypersensitivity in vivo in mice and that DRG derived from these mice had an increase (~4 fold) in TRPM8 mRNA ($P = 0.0006$) (**Fig. 3C**).[35] Importantly, DRG derived from mice tested with oxaliplatin followed by MTM rescue showed reversal of TRPM8 mRNA overexpression to baseline levels ($P = 0.001$).

Given our observations that MTM reversed oxaliplatin-induced cold hypersensitivity (**Figs. 2A–C**), we then validated our ability to pharmacologically block *TRPM8* and *TRPA1*, a TRP channel with conflicting reports of cold activation. As shown in (**Fig. 3D**), *TRPA1* antagonist HC-03003 completely blocked paw-licking behavior in response to AITC ($P = 0.015$) and *TRPM8* antagonist AMG333 inhibited icilin-induced "wet dog shakes" ($P = 0.0085$) (**Fig. 3E**). Then, we tested whether blockade of *TRPM8* or *TRPA1* would reverse oxaliplatin-induced cold hypersensitivity. As shown in **Fig. 3F**, the *TRPM8*-specific antagonist AMG333 reversed oxaliplatin-induced cold hypersensitivity (decreased paw withdrawal latency at 10°C) two hours post treatment ($P = 0.002$). Whereas, the *TRPA1* antagonist was without effect. Taken together, these findings support the hypothesis that MTM reversal of oxaliplatin-induced cold hypersensitivity is, in part, due to its ability to normalize *TRPM8* gene expression in DRG neurons under conditions of oxaliplatin-induced neurotoxicity.

3.6. Mithramycin induces apoptosis in ovarian cancer cell line OVCAR-3 and increases oxaliplatin-induced apoptosis in human colon cancer cell line HCT116

To further validate the activity of MTM used throughout this study, we sought to determine its anticancer (proapoptotic) properties in 2 established cancer models. First, we confirmed MTM's ability to induce apoptosis in the ovarian cancer cell line OVCAR3. Mithramycin at 50 nM, 200 nM, and 400 nM, increased apoptosis of OVCAR cells at 24 hours ($P < 0.0001$) as shown in

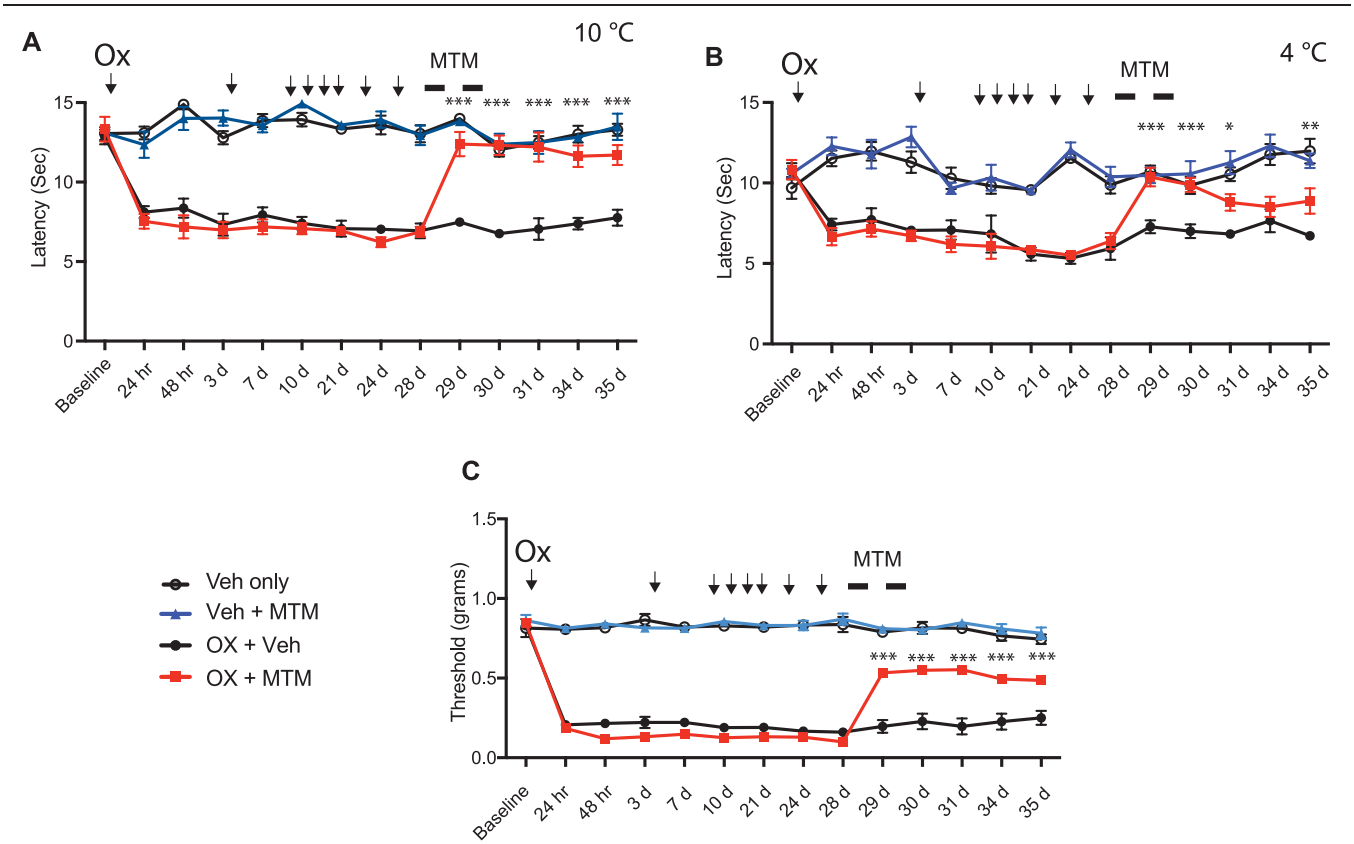

Figure 4. MTM reverses persistent oxaliplatin-induced cold and mechanical hypersensitivity. (A) Oxaliplatin (3 mg/kg ip) twice weekly for 4 weeks induced a persistent reduction in paw withdrawal latency to 10°C (cold hypersensitivity). MTM (100 μg/kg ip—bar) given on days 28 and 29 reversed cold hypersensitivity to near baseline values on days 29 to 35 (***$P < 0.0001$); n = 6. (B) MTM reversed oxaliplatin-induced hypersensitivity to 4°C on days 29 (***$P = 0.0004$), 30 (**$P = 0.0011$), 31 (*$P = 0.049$), and 35 (*$P = 0.025$); n = 6. (C) MTM produced a reversal of oxaliplatin-induced mechanical hypersensitivity on days 29 to 35 (***$P < 0.0001$); n = 6. There was no change in cold withdrawal latency or mechanical thresholds following MTM treatment alone. Statistical comparison: 2-way RM ANOVA with Tukey *post hoc* test. MTM, mithramycin; OX, oxaliplatin; RM, repeated-measures analysis of variance; Veh, vehicle.

Supplementary Figure 3, available at http://links.lww.com/PAIN/B865.[31] Subsequently, we examined the action of MTM in the presence of oxaliplatin. Oxaliplatin, a first-line treatment for metastatic colon cancer, mediates its cytotoxic action through complex mechanisms including disruption of DNA replication and apoptosis.[106] Although oxaliplatin-associated DNA adducts are maintained by covalent binding, concurrent treatment with MTM, a DNA binding transcriptional inhibitor,[65] may displace, disrupt, or compete with oxaliplatin's anticancer action. As literature to support or refute this possibility could not be identified, we tested whether MTM at 50 nM, a dose previously found to decrease *TRPV1* expression in DRG neurons in vitro,[108] would block oxaliplatin-induced apoptosis in a model of human colon cancer.[106] As shown in Supplementary Figure 3, available at http://links.lww.com/PAIN/B865, MTM increased apoptosis in the human colon cancer cell line HCT116 ($P < 0.0001$). Moreover, MTM (50 nM) with 10 or 20 μM oxaliplatin increased apoptosis in HCT116 cells in an additive manner ($P < 0.0001$). These findings support the suggestion that MTM used in our studies retains its anticancer activity[83] and complimented rather than blocked oxaliplatin's apoptotic activity in HCT116 cells.

3.7. Persistent oxaliplatin-induced cold and mechanical hypersensitivity is reversed by mithramycin

A progressive, dose- and cycle-dependent relationship occurs with the transition from acute to chronic cold- and mechanical-evoked pain following platinum-based chemotherapy. Therefore, cumulative exposure to oxaliplatin is associated with progressive increases in severity and duration (chronicity) of CIPN pain. To determine if MTM is able to reverse a persistent neuropathy model that is associated with cold and mechanical hypersensitivity following multiple oxaliplatin cycles, we treated mice with oxaliplatin (3 mg/kg) twice weekly for 4 weeks, followed by 2 doses of MTM

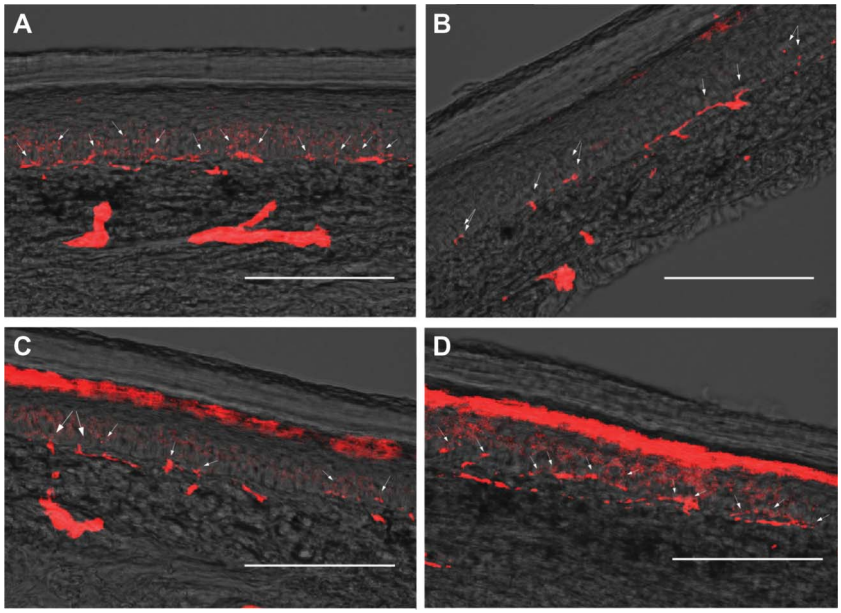

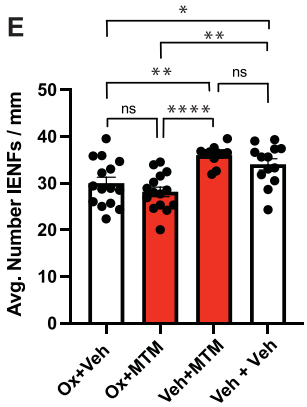

Figure 5. Intraepidermal nerve fiber (IENF) density of mouse skin following longer-term oxaliplatin administration with or without MTM rescue. Representative fluorescent images (arrows) of IENF visualized in mouse skin with anti-PGP9.5 targeted immunofluorescence (red) overlayed with corresponding bright field images (40X). (A) Vehicle-injected mice. (B) Mice treated twice weekly × 4 weeks with oxaliplatin. (C) Mice treated twice weekly with oxaliplatin × 4 weeks followed by MTM (100 μg/kg ip) on days 28 and 29. (D) Mice treated twice weekly with vehicle only × 4 weeks followed by MTM on days 28 and 29. Administration of oxaliplatin, MTM, and vehicle were exactly as described in Figure 4. Scale bars are 100 μm. (E) Quantitation of IENF density shows a decrease in IENF between OX vs Veh (*$P < 0.05$), OX vs MTM (**$P = 0.003$), OX + MTM vs MTM alone (****$P < 0.0001$), and OX + MTM vs Veh (**$P = 0.002$). Oxaliplatin (OX) = 3 mg/kg ip. MTM = 100 μg/kg ip. Image analysis is derived from 5 random sections from each mouse (n = 3) using 3 fields of view per sectionP. Statistical comparison: ANOVA with Tukey post hoc test. Mean ± SEM. ANOVA, analysis of variance; MTM, mithramycin; OX, oxaliplatin; Veh, vehicle.

(100 μg/kg). As shown in **Fig. 4A**, repeated injections of oxaliplatin decreased withdrawal latency to cold (10°C) from a baseline of 12.8 ± 0.5 seconds, to values that persisted through day 28 (6.9 ± 0.5 seconds). Following the first of the 2 MTM treatments (day 29), the persistent decrease in paw withdrawal latency reverted to baseline values (12.4 ± 0.8 seconds) that continued for the duration of the study period (1 week) until day 35 ($P < 0.0001$). Similar findings were observed (**Fig. 4B**) with MTM reversal of persistent oxaliplatin hypersensitivity evoked by a colder stimulus (4°C) with a decrease from baseline values of 10.7 ± 0.5 to 5.9 ± 0.7 seconds by day 28. Following MTM, latency values returned to baseline (10.4 ± 0.6 seconds) on day 29 ($P = 0.0004$) but maintained only a partial reversal on days 30 ($P = 0.0011$) and 31 ($P = 0.049$), until day 35 ($P = 0.025$).

In addition, mechanical threshold testing was performed following repeated doses of oxaliplatin resulting in a decrease from 0.83 ± 0.03 to 0.16 ± 0.03 g by day 28 (**Fig. 4C**). Following 2 MTM treatments, oxaliplatin mechanical hypersensitivity was reversed by approximately 50% for the duration of the study period with values of 0.49 ± 0.07 g by day 35 ($P < 0.0001$). Overall, the MTM-directed reversal of persistent cold (10°C and 4°C) and mechanical hypersensitivity, suggesting that certain

A

MGI Symbol	EnsemblGeneID	logFC	FDR
Sprr1a	ENSMUSG00000050359	-4.31	3.79E-08
Ecel1	ENSMUSG00000026247	-3.04	8.34E-09
Npy	ENSMUSG00000029819	-2.10	5.54E-03
Atf3	ENSMUSG00000026628	-1.61	8.91E-08
Car1	ENSMUSG00000027556	-1.44	1.03E-06
Ermap	ENSMUSG00000028644	-1.37	2.72E-04
Nts	ENSMUSG00000019890	-1.37	8.34E-09
Oas3	ENSMUSG00000032661	-1.36	6.90E-10
Gpr151	ENSMUSG00000042816	-1.20	4.47E-05
Ctse	ENSMUSG00000004552	-1.12	2.99E-03
Hemgn	ENSMUSG00000028332	-1.08	5.06E-03
Usp18	ENSMUSG00000030107	-1.00	1.23E-03
Epb42	ENSMUSG00000023216	-0.89	1.46E-02
Sectm1b	ENSMUSG00000039364	-0.88	1.23E-06
Zbp1	ENSMUSG00000027514	-0.87	3.38E-03
Ifit1	ENSMUSG00000034459	-0.87	1.75E-02
Slc12a3	ENSMUSG00000031766	-0.83	1.02E-04
Gm4869	ENSMUSG00000106350	-0.83	7.05E-05
Gfap	ENSMUSG00000020932	-0.79	9.60E-04
Tmem88b	ENSMUSG00000073680	-0.77	3.90E-02
Gm42970	ENSMUSG00000106446	-0.77	1.59E-04
Gm29266	ENSMUSG00000101797	-0.76	1.34E-03
Gm49268	ENSMUSG00000115131	-0.75	2.29E-04
Nlrc5	ENSMUSG00000074151	-0.74	8.09E-04
Gm13187	ENSMUSG00000087355	-0.73	5.41E-03
Cdc6	ENSMUSG00000017499	-0.73	9.53E-03
H2bc7	ENSMUSG00000069268	-0.72	5.39E-03
Gm48239	ENSMUSG00000114230	-0.71	1.48E-04
Oas2	ENSMUSG00000032690	-0.71	2.92E-03
Sox11	ENSMUSG00000063632	-0.71	4.48E-05
Loxl4	ENSMUSG00000025185	-0.71	1.55E-03
Avpr1a	ENSMUSG00000020123	-0.70	3.32E-02
Gm50368	ENSMUSG00000117895	-0.69	1.27E-02
Tecta	ENSMUSG00000037705	-0.69	7.46E-10

MGI Symbol	EnsemblGeneID	logFC	FDR
Adam8	ENSMUSG00000025473	-0.69	1.56E-07
Gm45591	ENSMUSG00000109460	-0.68	1.01E-02
Gm47197	ENSMUSG00000111155	-0.67	2.99E-03
Vgf	ENSMUSG00000037428	-0.67	1.59E-04
Ms4a6d	ENSMUSG00000024679	-0.66	2.67E-02
Sting1	ENSMUSG00000024349	-0.65	2.67E-03
Ifi213	ENSMUSG00000073491	-0.65	1.07E-02
Gm22513	ENSMUSG00000096349	-0.64	4.25E-02
Gm17137	ENSMUSG00000090559	-0.64	1.37E-02
D630030B08Rik	ENSMUSG00000106837	-0.64	2.48E-03
Gm39041	ENSMUSG00000108460	-0.63	1.27E-02
H2bc3	ENSMUSG00000075031	-0.62	2.56E-02
Steap1	ENSMUSG00000015652	-0.62	1.43E-02
Isg15	ENSMUSG00000035692	-0.61	2.92E-02
Gm42879	ENSMUSG00000106590	-0.60	1.92E-03
Gm43502	ENSMUSG00000106537	-0.59	1.46E-03
Alkal2	ENSMUSG00000054204	-0.59	4.98E-03
Gm43776	ENSMUSG00000105946	-0.59	4.43E-03
Top2a	ENSMUSG00000020914	-0.58	2.21E-02
Gm10862	ENSMUSG00000104284	-0.58	1.31E-02
Dnase1l3	ENSMUSG00000025279	-0.58	1.21E-08
Gm48804	ENSMUSG00000112596	-0.58	8.71E-03
Gm48267	ENSMUSG00000114624	-0.58	2.06E-02
Rnf17	ENSMUSG00000000365	0.58	4.43E-02
Vmn1r85	ENSMUSG00000070817	0.59	1.87E-02
Vwde	ENSMUSG00000079679	0.59	1.77E-03
Hmgn5	ENSMUSG00000031245	0.59	1.78E-02
Tpsb2	ENSMUSG00000033825	0.61	4.97E-04
Zfp804b	ENSMUSG00000092094	0.64	6.99E-03
Cep290	ENSMUSG00000019971	0.64	8.98E-03
Syt13	ENSMUSG00000027220	0.65	1.60E-03
Rbp4	ENSMUSG00000024990	0.69	2.15E-02
Gm14412	ENSMUSG00000078868	0.70	5.63E-04
Slc10a2	ENSMUSG00000023073	0.94	1.07E-06
Vdac3-ps1	ENSMUSG00000075053	1.22	1.27E-02

B

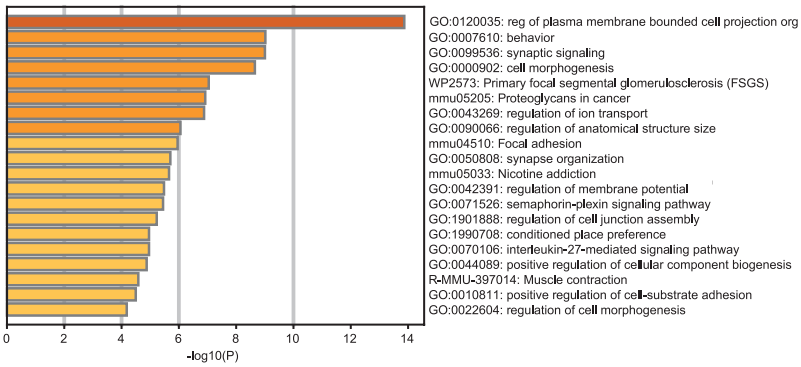

C

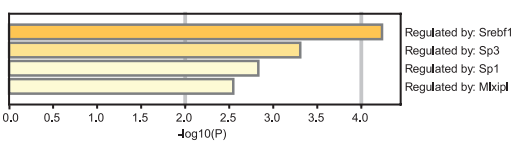

Figure 6. Oxaliplatin-induced differentially expressed genes and enriched pathways in DRG. (A) Top differentially expressed genes (DEGs) with vehicle only (vehicle + vehicle = VV) as base, compared with oxaliplatin-only (oxaliplatin + vehicle) treatment. Downregulated (blue) and upregulated (red) DEGs are shown. FDR <0.05, logFC > 0.38 (fold change greater than 1.5). (B) Enrichment analysis of OX-treated DRG (Metascape) using ontology sources: GO Biological Processes, KEGG Pathway, Reactome Gene Sets, CORUM, PaGenBase, WikiPathways, and PANTHER Pathway. Log10(P) is the *P* value in log base 10. (C) Enrichment analysis of OX-treated DRG by TRRUST (Transcriptional Regulatory Relationships Unraveled by Sentence – based Text mining (https://www.grnpedia.org/trrust/). DRG, dorsal root ganglion.

sustained transcription-dependent changes induced by oxaliplatin are shared by cold and mechanical sensory transduction and can be reversed by an inhibitor of Sp1-like factors.

3.8. Mithramycin does not reverse oxaliplatin-induced decreases in intraepidermal nerve fiber density

Several chemotherapeutic agents, such as oxaliplatin, induce peripheral neuropathy.[14] A decrease in intraepidermal nerve fiber (IENF) density was reported in mice 4 weeks after paclitaxel treatment[10]; after 11 weeks of oxaliplatin (3 mg/kg × 10 doses over 3 weeks)[103]; and at 30 days in humans (3 doses of oxaliplatin): 3 of 8 patients had a decreased IENF density that at day 180 was more pronounced.[14] Given this variability, the relationship between chemotherapy-induced reduction of IENF density and painful hypersensitivity remains an open question. Therefore, we investigated whether MTM treatment (2 doses), which reversed persistent cold and mechanical hypersensitivity, would also reverse oxaliplatin-induced reduction in IENF density. As shown in **Figs. 5A–E**, long-term oxaliplatin treatment (8 doses over 4 weeks) reduced IENF density (30 ± 1.3 IENF/mm), compared with vehicle control (34.0 ± 1.2 IENF/mm) ($P < 0.05$). Although MTM reversed persistent oxaliplatin-induced cold and mechanical hypersensitivity (**Fig. 4**), MTM failed to reverse the oxaliplatin-induced IENF loss during the same period of our investigation (7 days following the first MTM treatment) (28.1 ± 1.0 IENF/mm) ($P = 0.002$). When compared with vehicle, MTM treatment alone did not change the IENF density (36 ± 0.6 IENF/mm). Moreover, oxaliplatin plus vehicle ($P = 0.003$) or oxaliplatin plus MTM ($P < 0.0001$) compared with MTM alone were both associated with persistent reduction in IENF density.

3.9. Oxaliplatin induces genome wide transcriptional changes within dorsal root ganglion

Although oxaliplatin-induced transcriptional inhibition represents a fundamental mechanism underlying its anticancer activity,[3] how oxaliplatin binding to the DRG genome results in painful CIPN remains poorly understood. Therefore, we undertook an extensive analysis of the transcriptional changes induced by oxaliplatin in the DRG to identify not only potential genes of interest but also to establish a framework of gene networks that may underlie oxaliplatin-induced painful hypersensitivity. Lumbar DRG RNA was extracted from mice treated with only oxaliplatin (oxaliplatin + vehicle OV) and compared with DRG RNA from vehicle-only DRG RNA (vehicle + vehicle VV). A total of 931 DEGs were identified (FDR < 0.05). The top DEGs with a log fold change of ±0.38 (fold change for ±1.5) are displayed in **Fig. 6A**. A complete table of the DEGs is shown in Supplementary Table 1, available at http://links.lww.com/PAIN/B864. Assuming the transcriptome of

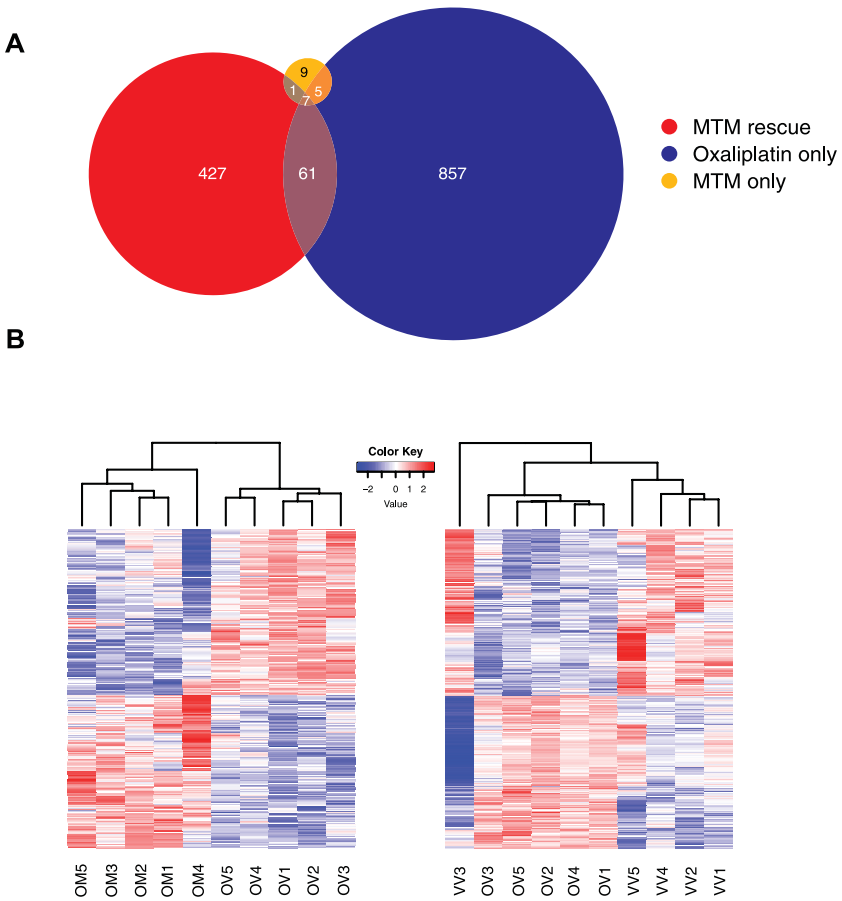

Figure 7. Transcriptional changes in DRG because of oxaliplatin and MTM treatment. (A) Venn diagram showing differentially expressed genes (DEGs) (FDR <0.05) and their overlap between oxaliplatin (OX) treatment (blue = 930 genes), OX plus MTM (red = 496 genes), and MTM alone (orange = 22 genes). Only a small fraction of DEGs (61) overlap between OX alone vs OX + MTM. (B) Heat map shows transcriptional changes because of OX alone (OV1-5) vs vehicle only (VV1-5). Heat map of DEGs derived from OX + MTM (OM1-5) vs OX treatment alone (OV1-5). Distinct genes are upregulated (red) and conversely downregulated (blue) between treatment groups. Color key indicates logFC. MTM, mithramycin; DRG, dorsal root ganglion.

approximately 30,000 genes, approximately 3% of genes showed significant changes. This finding suggests broad changes in gene expression occurred following the administration of oxaliplatin.

Two prior studies used RNAseq to examine the DRG transcriptomic changes because of oxaliplatin treatment.[5,98] The DEGs from our oxaliplatin-only (OV) were compared with DEGs from these studies. When compared with the data published from Starobova et al.,[98] only 7 genes appeared in our data set (ie, A330023F24Rik, Cadm2, Gm26871, Meg3, Nav2, Zbtb33, and Zfp804a). It is worth noting that Starobova et al. used intraplantar injection of oxaliplatin to induce a

A

MGI Symbol	EnsemblGeneID	logFC	FDR
Gm24305	ENSMUSG00000095590	-2.03	1.13E-02
Slc4a1	ENSMUSG00000006574	-1.10	7.84E-03
Gm14440	ENSMUSG00000078901	-1.09	8.22E-03
Spta1	ENSMUSG00000026532	-1.06	1.76E-02
Gm42047	ENSMUSG00000110631	-0.99	1.06E-05
Hba-a1	ENSMUSG00000069919	-0.95	4.92E-03
Ctse	ENSMUSG00000004552	-0.92	3.88E-02
Gypa	ENSMUSG00000051839	-0.92	2.34E-02
Gm6878	ENSMUSG00000075549	-0.87	8.13E-04
H2bc15	ENSMUSG00000095217	-0.82	3.07E-03
Gm49980	ENSMUSG00000117465	-0.82	8.20E-04
Hbb-bs	ENSMUSG00000052305	-0.82	2.39E-02
Tpsb2	ENSMUSG00000033825	-0.80	3.77E-05
Gm11960	ENSMUSG00000081974	-0.79	3.69E-03
Hba-a2	ENSMUSG00000069917	-0.78	1.73E-02
Ubxn11	ENSMUSG00000012126	-0.66	4.59E-02
Gsdmd	ENSMUSG00000022575	-0.61	3.66E-02
Gm12286	ENSMUSG00000081600	-0.59	5.25E-03
Gm23973	ENSMUSG00000065254	-0.58	2.87E-05
Tent5c	ENSMUSG00000044468	-0.56	1.22E-02
Gbp6	ENSMUSG00000104713	-0.56	3.22E-02
Lypd2	ENSMUSG00000022595	-0.56	4.50E-02
Pamr1	ENSMUSG00000027188	-0.55	1.01E-02
Cd79a	ENSMUSG00000003379	-0.55	2.92E-02
Gm25117	ENSMUSG00000087819	-0.53	2.92E-02
Adam1a	ENSMUSG00000072647	-0.51	4.81E-02
Bub1b	ENSMUSG00000040084	-0.51	3.29E-02
Clec7a	ENSMUSG00000079293	-0.51	2.53E-02
Gm43197	ENSMUSG00000107215	-0.49	4.35E-02
Gm43305	ENSMUSG00000105703	-0.48	4.81E-02
Ccr5	ENSMUSG00000079227	-0.48	3.72E-02
Edn3	ENSMUSG00000027524	-0.48	2.53E-02
Rasgrp2	ENSMUSG00000032946	-0.47	9.44E-03
Itih2	ENSMUSG00000037254	-0.47	4.41E-02
Dock2	ENSMUSG00000020143	-0.46	9.46E-04
Fibin	ENSMUSG00000074971	-0.43	3.72E-02
Hhip	ENSMUSG00000064325	-0.42	8.00E-03
Cx3cr1	ENSMUSG00000052336	-0.41	4.51E-02
Etv4	ENSMUSG00000017724	-0.40	2.87E-02
Svep1	ENSMUSG00000028369	-0.38	1.06E-05
Naa38	ENSMUSG00000059278	-0.38	8.22E-03
Rpl10a-ps1	ENSMUSG00000084416	0.38	2.94E-05
Pkib	ENSMUSG00000019876	0.38	4.17E-07

MGI Symbol	EnsemblGeneID	logFC	FDR
Gm37509	ENSMUSG00000104379	0.38	4.36E-02
Gm10288	ENSMUSG00000070343	0.39	2.25E-02
Gm28437	ENSMUSG00000101111	0.39	3.23E-03
Sdc1	ENSMUSG00000020592	0.39	4.74E-03
Mindy4b-ps	ENSMUSG00000101860	0.40	2.94E-05
Gm28438	ENSMUSG00000101939	0.40	1.74E-03
Il31ra	ENSMUSG00000050377	0.41	7.96E-03
Gm8960	ENSMUSG00000112099	0.41	7.64E-03
BC085271	ENSMUSG00000102478	0.41	4.89E-03
Gm10221	ENSMUSG00000067719	0.42	4.09E-02
Fam107a	ENSMUSG00000021750	0.42	3.30E-02
Gm11966	ENSMUSG00000080904	0.43	3.85E-03
mt-Atp8	ENSMUSG00000064356	0.45	2.94E-05
Gm13772	ENSMUSG00000080977	0.45	5.82E-03
Rps2-ps10	ENSMUSG00000091957	0.46	3.78E-02
Gm41442	ENSMUSG00000116946	0.49	1.36E-04
Mt1	ENSMUSG00000031765	0.49	2.68E-05
Gm48697	ENSMUSG00000111995	0.51	1.60E-02
Plk5	ENSMUSG00000035486	0.51	3.10E-02
Serpina3i	ENSMUSG00000079014	0.51	1.36E-05
Sox11	ENSMUSG00000063632	0.53	1.37E-03
Gm10222	ENSMUSG00000067736	0.54	1.80E-08
Gm14296	ENSMUSG00000074527	0.55	2.01E-02
mt-Nd4l	ENSMUSG00000065947	0.55	3.75E-08
Smr2	ENSMUSG00000029281	0.55	1.04E-03
Olfr920	ENSMUSG00000061039	0.57	1.33E-05
Gm2805	ENSMUSG00000116536	0.58	1.10E-02
Nnat	ENSMUSG00000067786	0.58	9.03E-05
Gm17149	ENSMUSG00000090334	0.59	2.27E-02
Pdk4	ENSMUSG00000019577	0.59	6.02E-03
Tmem88b	ENSMUSG00000073680	0.60	2.27E-02
Gm7105	ENSMUSG00000118345	0.61	7.73E-03
Gm5526	ENSMUSG00000084817	0.69	1.04E-03
Gm4869	ENSMUSG00000106350	0.70	1.71E-02
Gpr151	ENSMUSG00000042816	0.75	2.25E-02
Mt2	ENSMUSG00000031762	0.82	3.48E-04
Sectm1b	ENSMUSG00000039364	0.85	1.11E-03
Atf3	ENSMUSG00000026628	0.95	1.55E-03
Nts	ENSMUSG00000019890	1.15	8.88E-13
Ecel1	ENSMUSG00000026247	2.15	2.85E-08
Trim30a	ENSMUSG00000030921	2.61	3.67E-05
Sprr1a	ENSMUSG00000050359	3.02	1.91E-11
Gm23804	ENSMUSG00000094826	4.21	4.73E-08

B

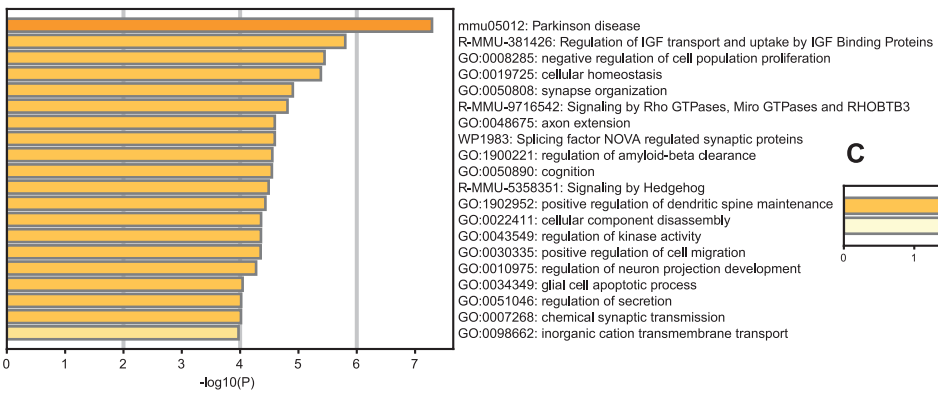

C

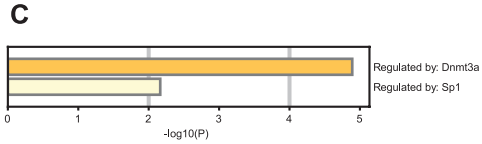

Figure 8. Mithramycin-rescue of differentially expressed genes and enriched pathways in DRG. (A) Top differentially expressed genes (DEGs) with oxaliplatin-only (oxaliplatin + vehicle = OV) as base, compared with oxaliplatin + mithramycin (OM) treatment. Downregulated (blue) and upregulated (red) DEGs are shown. FDR <0.05, logFC > 0.38 (fold change greater than 1.5). (B) Enrichment analysis of MTM-rescue DRG (Metascape) using ontology sources: GO Biological Processes, KEGG Pathway, Reactome Gene Sets, CORUM, PaGenBase, WikiPathways and PANTHER Pathway. Log10(P) is the *P* value in log base 10. (C) Enrichment analysis of MTM-rescue DRG by TRRUST (Transcriptional Regulatory Relationships Unraveled by Sentence–based Text mining (https://www.grnpedia.org/trrust/). DRG, dorsal root ganglion; MTM, mithramycin.

hypersensitive state; by contrast, our studies used systemic administration. When compared with the data published from Bangash et al.,[5] using microarray assays for gene expression quantification, no overlapping genes were found between data sets representing oxaliplatin-treatment alone. We suggest that a combination of systemic oxaliplatin treatment and an RNA sequencing depth of approximately 50 million reads facilitated the identification of a greater number of transcriptomic changes than previously reported. As such, our data serve as an ongoing resource for the study of transcriptional changes that occur within the DRG because of oxaliplatin treatment in vivo.

As shown in **Fig. 6B**, using DEGs derived from oxaliplatin-treated mouse DRG, an accumulative hypergeometric statistical analysis was used to identify the ontological terms where the input genes show significant enrichment. This enrichment analysis revealed functional associations among the DEGs including the regulation of plasma membrane projection organization, behaviors, synaptic signaling, and cell morphogenesis. Analysis of which putative transcription factor(s) regulate the oxaliplatin-induced DEGs revealed 2 members (Sp1, Sp3) of the Sp1-like transcription factor family (**Fig. 6C**). Sp1 and Sp4 are drivers of *TRPV1* promoter activity and *TRPV1* expression in DRG neurons[20] with member Sp4 being necessary for the persistence of oxaliplatin-induced hypersensitivity.[90]

3.10. Mithramycin reversal of oxaliplatin-induced hypersensitivity is associated with transcriptional changes only partially overlapping those induced by oxaliplatin

As shown in **Fig. 7A**, a Venn diagram illustrates the distribution of DEGs between oxaliplatin treatment only (OV), mithramycin rescue of oxaliplatin treatment (OM) and MTM only (VM). Of the 496 DEGs from the mithramycin rescue group, only 61 genes overlap with the oxaliplatin-only condition. Mithramycin treatment alone is associated with only 22 DEGs. Therefore, the majority of transcriptional changes observed with MTM-mediated reversal of painful hypersensitivity are not associated with oxaliplatin-induced DEGs. Heat maps of these DEGs are shown in **Fig. 7B**.

The top MTM-associated DEGs are shown in **Fig. 8A**, and a complete list of oxaliplatin + MTM rescue DEGS are listed in Supplementary Table 2, available at http://links.lww.com/PAIN/B864. Ontology enrichment analysis of MTM rescue DEGs (**Fig. 8B**) show top functional associations with Parkinson disease, transport and uptake of IGF, regulation of cellular proliferation, cellular homeostasis, and synapse organization. Notably, analysis of how putative transcription factor(s) regulate the MTM rescue–associated DEGs revealed two: Dnmt3a and Sp1. DNA methylase 3a (Dnmt3a) was found to be associated with neuropathic pain through repression of KCNa2 in primary afferent neurons.[110] Sp1 is the well-described target of MTM—its principal inhibitor of DNA binding to GC-rich promoter sites. The 61 DEGs overlapping between oxaliplatin only and MTM rescue are shown in Supplementary Figure 4, available at http://links.lww.com/PAIN/B865. Although a survey of these DEGs (PubMed) revealed several individual pain-related genes, no overall thematic pattern of gene function was appreciated.

3.11. Mithramycin reversal is associated with differentially expressed genes whose function are at multiple levels of known nociceptor function

To better understand the potential function of the DEGs underlying MTM reversal of painful hypersensitivity at the level

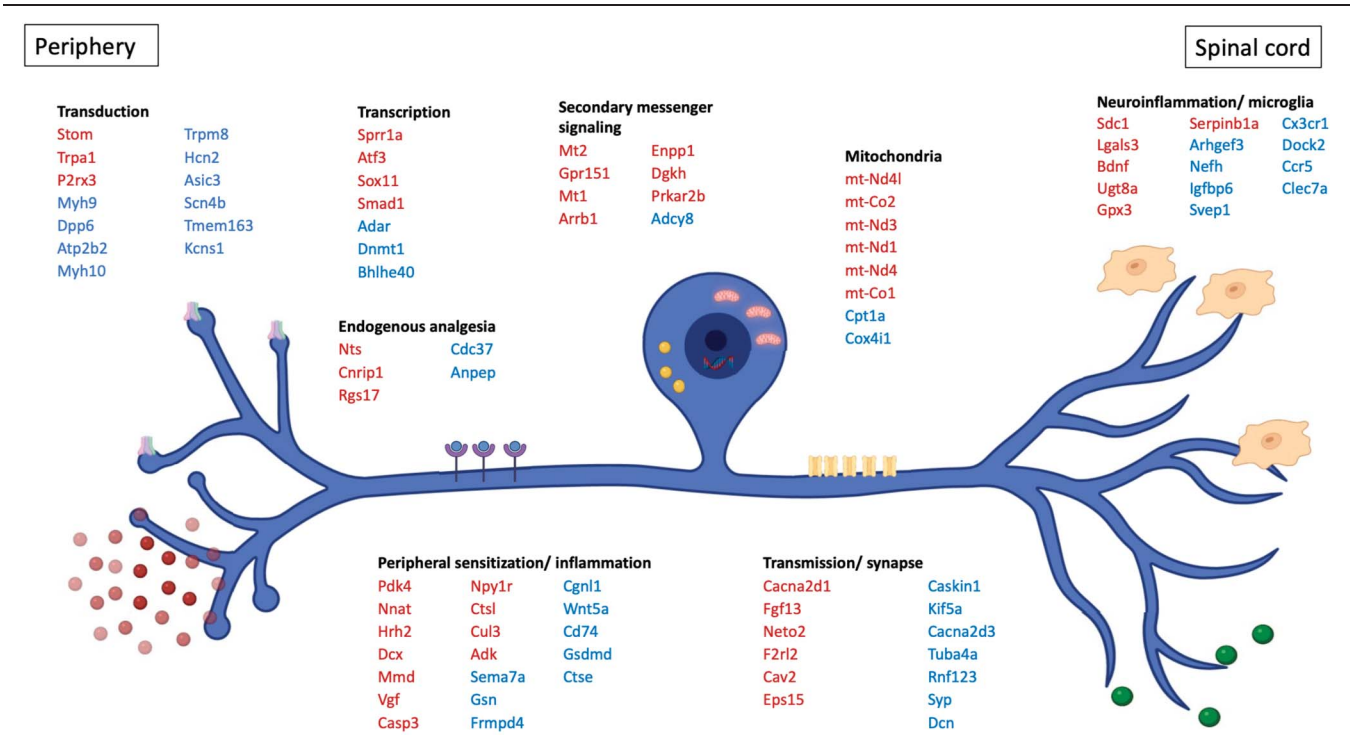

Figure 9. Model of primary afferent nociceptor expressing differentially expressed genes (DEGs) identified from MTM rescue of oxaliplatin-induced hypersensitive state. The DRG MTM treatment group (OM) was used as input for database mining to ascribe a putative categorization from publicly available pain gene databases including previous studies[53,58,73] and the Pain Research Forum - Pain Gene Resource and automated text-based Medline searches (easyPubmed package in R). Downregulated (blue) and upregulated (red) genes are shown. DRG, dorsal root ganglion; MTM, mithramycin.

of molecular nociception, we compared these genes with known pain gene databases and searched in a semiautomated manner through a PubMed query. Differentially expressed genes with known association with pain were putatively assigned a category of function as depicted in **Fig. 9**. References that support these categorizations are found in Supplementary Table 3, available at http://links.lww.com/PAIN/B864. Based on this categorization of MTM reversal–associated DEGs, we hypothesize that these MTM-regulated genes modulate nociceptor function at multiple levels through transcription, transduction, and transmission.

3.12. Protein-protein enrichment analysis of mithramycin reversal identifies mitochondrial electron transport chain genes as a potential therapeutic target

Using the list of DEGs identified through the analysis of the MTM reversal group, a further enrichment analysis was performed at the level of their protein products. By evaluating DEGs at this level, protein–protein interaction network analysis can identify biologically relevant pathways/processes with a better signal-to-noise ratio than the ontological enrichment analysis of RNA transcript levels alone. The Metascape tool uses a network analysis algorithm (the molecular complex detection algorithm—MCODE[4]) to cluster DEGs with highly associated protein–protein interactions. As shown in **Fig. 10**, genes that have significant protein–protein interactions are related to the function of the mitochondrial electron transport chain (ETC)—oxidative phosphorylation, MCODE 5 (see boxed regions) (**Fig. 10**). Additional DEGs related to mitochondrial function under conditions of MTM reversal or oxaliplatin treatment are shown in Supplementary Figure 5, available at http://links.lww.com/PAIN/B865.[100] Overall, these MCODE5-identified genes include principal components of ETC's Complex 1: NADH dehydrogenase (ND1, ND3, ND4, ND4L, NDufa6, Ndufb6)[111] that is a critical production site for pathological reactive oxygen species (ROS).[57] Given that mitochondrial ROS production is known to serve a critical role in neuronal signaling, nociceptor function, and hypersensitivity, we sought to link this protein–protein interaction analysis to potential mechanisms driving both oxaliplatin-induced hypersensitivity and its reversal by MTM in vivo.

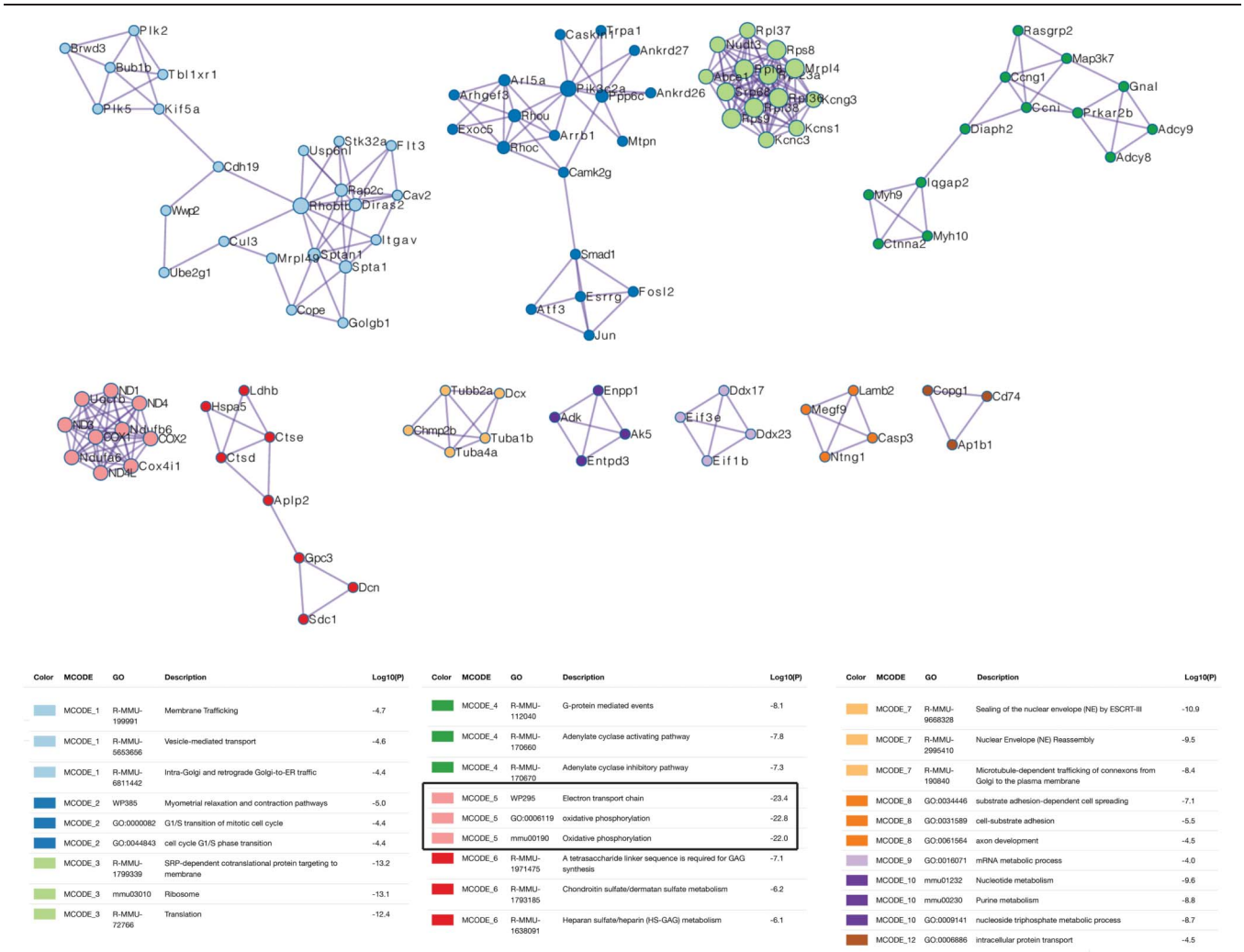

Color	MCODE	GO	Description	Log10(P)
	MCODE_1	R-MMU-199991	Membrane Trafficking	-4.7
	MCODE_1	R-MMU-5653656	Vesicle-mediated transport	-4.6
	MCODE_1	R-MMU-6811442	Intra-Golgi and retrograde Golgi-to-ER traffic	-4.4
	MCODE_2	WP385	Myometrial relaxation and contraction pathways	-5.0
	MCODE_2	GO:0000082	G1/S transition of mitotic cell cycle	-4.4
	MCODE_2	GO:0044843	cell cycle G1/S phase transition	-4.4
	MCODE_3	R-MMU-1799339	SRP-dependent cotranslational protein targeting to membrane	-13.2
	MCODE_3	mmu03010	Ribosome	-13.1
	MCODE_3	R-MMU-72766	Translation	-12.4

Color	MCODE	GO	Description	Log10(P)
	MCODE_4	R-MMU-112040	G-protein mediated events	-8.1
	MCODE_4	R-MMU-170660	Adenylate cyclase activating pathway	-7.8
	MCODE_4	R-MMU-170670	Adenylate cyclase inhibitory pathway	-7.3
	MCODE_5	WP295	Electron transport chain	-23.4
	MCODE_5	GO:0006119	oxidative phosphorylation	-22.8
	MCODE_5	mmu00190	Oxidative phosphorylation	-22.0
	MCODE_6	R-MMU-1971475	A tetrasaccharide linker sequence is required for GAG synthesis	-7.1
	MCODE_6	R-MMU-1793185	Chondroitin sulfate/dermatan sulfate metabolism	-6.2
	MCODE_6	R-MMU-1638091	Heparan sulfate/heparin (HS-GAG) metabolism	-6.1

Color	MCODE	GO	Description	Log10(P)
	MCODE_7	R-MMU-9668328	Sealing of the nuclear envelope (NE) by ESCRT-III	-10.9
	MCODE_7	R-MMU-2995410	Nuclear Envelope (NE) Reassembly	-9.5
	MCODE_7	R-MMU-190840	Microtubule-dependent trafficking of connexons from Golgi to the plasma membrane	-8.4
	MCODE_8	GO:0034446	substrate adhesion-dependent cell spreading	-7.1
	MCODE_8	GO:0031589	cell-substrate adhesion	-5.5
	MCODE_8	GO:0061564	axon development	-4.5
	MCODE_9	GO:0016071	mRNA metabolic process	-4.0
	MCODE_10	mmu01232	Nucleotide metabolism	-9.6
	MCODE_10	mmu00230	Purine metabolism	-8.8
	MCODE_10	GO:0009141	nucleoside triphosphate metabolic process	-8.7
	MCODE_12	GO:0006886	intracellular protein transport	-4.5

Figure 10. Components of DRG mitochondrial electron transport chain (ETC) are negatively regulated by MTM rescue of oxaliplatin-induced hypersensitivity. Protein–protein interaction enrichment analysis (Metascape) of oxaliplatin (OX) + MTM using databases: STRING, BioGrid, OmniPath, InWeb IM, and the Molecular Complex Detection (MCODE) algorithm, identified MCODE module 5 (ETC) as the best scoring terms by *P* value (see boxed values for ETC module Log10P). DRG, dorsal root ganglion; MTM, mithramycin.

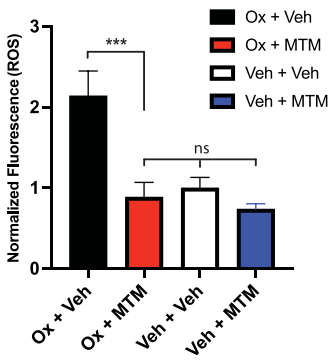

Figure 11. Mithramycin (MTM) reverses in vivo oxaliplatin-induced DRG neuronal production of reactive oxygen species (ROS). Normalized ROS fluorescence (ROS cell mean GFP * ROS cell #)/(Cell mean GFP * Cell #) ex vivo measured from DRG neurons cultured on day 10 following in vivo treatment of mice with Ox + Veh (3 mg/kg, i.p.) on day 0, MTM + Veh (100 μg/kg, i.p.) on day 2 and day 3 and harvested on day 10. MTM reversed the OX-induced 2.2-fold increase in ROS in DRG neurons (*** $P = 0.0004$; ns = not significant); n = 3 independent experiments, each with 3 replicate culture. Statistical comparison: ordinary one-way ANOVA, Tukey post hoc test. Mean values ± SEM. ANOVA, analysis of variance; DRG, dorsal root ganglion.

3.13. Mithramycin reverses oxaliplatin-induced increases of reactive oxygen species in dorsal root ganglion neurons

Excessive ROS generation induced by platinum agents such as oxaliplatin, that leads to oxidative stress and mitochondrial dysfunction, contribute to the development of CIPN.[45,76] DRG neurons exposed to oxaliplatin in vitro induced a dose-dependent and time-dependent mitochondrial production of ROS.[50,63] Given the observed enrichment of ETC components following MTM rescue, we investigated whether DRG neurons increased their content of ROS in response to oxaliplatin treatment in vivo and if MTM treatment could reverse this effect. As shown in **Fig. 11**, ROS levels were significantly increased in DRG neurons derived from oxaliplatin-treated mice (2.2 ± 0.47) 10 days after oxaliplatin treatment as compared with those from vehicle-treated mice (1.0 ± 0.10) ($P = 0.0004$). Although MTM (100 μg/kg, i.p.) treatment alone on day 2 and day 3 did not significantly change ROS levels, DRG neurons cultured from oxaliplatin-treated mice and subsequently with MTM on days 2 and 3 displayed ROS levels of 0.83 ± 0.09 on day 10 that did not differ from baseline to control values. We propose that as a component of its transcriptional effects in DRG neurons, MTM reversal of oxaliplatin-induced ROS overproduction underlies, in part, MTM reversal of painful hypersensitivity to oxaliplatin.

3.14. Differential alternative splice analysis reveals cytoskeletal-dependent transport genes as a major site of mithramycin regulation in oxaliplatin treated dorsal root ganglion

Analysis of gene expression as measured by DEGs alone may limit our understanding of the complexity of oxaliplatin-induced and MTM-induced changes across the DRG genome. Differential alternative RNA splicing is another critical component in the regulation of gene expression.[101] We designed our RNAseq experiments for a depth of approximately 50 million reads per sample allowing for differential splice analysis using the established rMATs package.[91] At this deeper depth of read, we aimed to identify important splice changes in gene families and pathways that may otherwise go undetected.

There were 2313 differential splice events across 1533 genes with the MTM reversal and oxaliplatin treatment groups. The principal component plot (PCA) (**Fig. 12A**) shows the first principal component (x-axis) in the dimension where there is the greatest variance (PC1 39.9%). As the red (MTM rescue) and blue (oxaliplatin only) conditions have the largest separation in this dimension, we interpret that MTM treatment contributes the greatest variance in splicing between the groups. Overall, the represented differential splicing is occurring within the same gene(s). However, the proposed spliced isoforms are different between the 2 treatment groups (MTM rescue vs oxaliplatin only).

Based on the identification of differences in the splice events of individual genes driven by MTM treatment, an ontological enrichment pathway analysis of the differentially alternatively spliced genes was conducted to identify pathways enriched for differential splicing events. Most of the differentially spliced genes have a function related to cytoskeletal-dependent transport, synaptic organization, and cytosolic transport that overall align with axonal transport (**Fig. 12B**). As axonal transport was identified as a key mechanism for CIPN, these differential splicing events may represent early changes that contribute to CIPN.[52]

4. Discussion

We tested the hypothesis that mithramycin-mediated reversal of painful hypersensitive states is dependent on the regulation of nociceptive genes and gene families expressed in peripheral sensory neurons.

4.1. Reversal of inflammatory and neuropathic pain by mithramycin

Inflammation induced by localized injection of CFA produced heat hyperalgesia in male mice that was completely reversed by MTM (**Figs. 1A and D**). Similarly, MTM reversed cisplatin-induced heat hyperalgesia (**Fig. 1E**). Both are *TRPV1*-dependent processes.[15,26,78,99] These observations support our prior findings that MTM blocked *TRPV1* expression through Sp1- and Sp4-dependent mechanisms.[20] In addition, MTM treatment of DRG neurons in vitro reduced the number of capsaicin-responsive DRG neurons rather than their response magnitude.[108] These findings suggest that MTM in vivo decreased the expression of *TRPV1* in a subset of sensory neurons that are dependent on Sp1-like transcription factors. Sp4 is expressed predominantly in smaller-diameter DRG neurons and is critical for the maintenance of CFA-induced painful hypersensitive states.[90] We hypothesize that the action of MTM under inflammatory and cisplatin conditions is directed at this dynamic subpopulation of DRG neurons by reversing aberrant Sp4- and/or Sp1-dependent neuroplastic changes in the DRG genome. Therefore, ongoing expression of *TRPV1* in sensory neurons lacking Sp1-like regulation would be insensitive to MTM's action. This model may explain why we observed no difference in baseline heat withdrawal latencies in $Sp4^{+/-}$-knockout mice, whereas $TRPV1^{-/-}$-null mice had higher heat withdrawal latencies.[90]

The platinum-based chemotherapy oxaliplatin, used to treat metastatic colon cancer, is associated with significant dose-limiting neuropathic side effects, including cold allodynia and hyperalgesia that are poorly understood.[75] We observed MTM reversal of oxaliplatin cold hypersensitivity without a change in

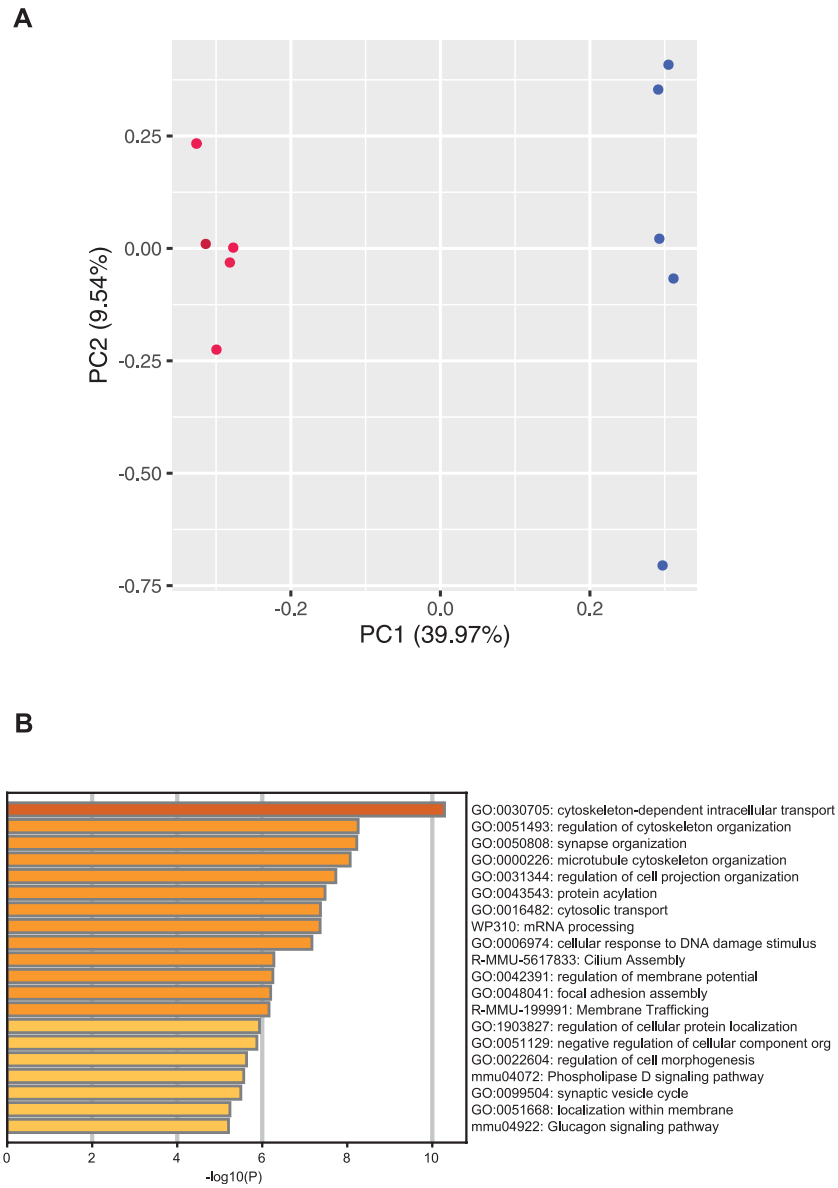

Figure 12. Mithramycin (MTM) rescue of oxaliplatin-induced hypersensitivity reveals a unique cohort of DRG spliced genes. (A) Principal component analysis (PCA) plot of splice events across 1533 OM and OV genes is shown. Red indicates MTM rescue group, and blue indicates OX treatment only. Differential alternative splicing analysis performed by RMAT.[91] (B) Enrichment analysis identified differentially spliced genes dedicated to cytoskeleton intracellular transport and synaptic regulation as top pathways associated with MTM rescue in DRG. Databases (Metascape): GO Biological Processes, KEGG Pathway, Reactome Gene Sets, CORUM, PaGenBase, WikiPathways, and PANTHER Pathway. Log10(P) is the *P*-value in log base 10. DRG, dorsal root ganglion.

control baseline withdrawal latencies (**Figs. 2B and C**).[77] Multiple mechanisms have been examined to both understand and develop effective therapies for oxaliplatin-induced painful CIPN,[1,27,68] including the role of TRPM8.[67,68] Our studies, support the hypothesis that MTM reverses oxaliplatin-induced cold hypersensitivity (**Figs. 2A–C**) by normalization of *TRPM8* gene expression in nociceptors (**Fig. 3**).

When compared with male mice, the observations that female mice exhibited a greater CFA-induced heat hyperalgesia (**Fig. 1C**) but lower efficacy of MTM reversal of hypersensitivity (Supplementary Figure 2, available at http://links.lww.com/PAIN/B865) suggests sex differences in genes regulated by Sp1-like factors. Although other factors may help explain these findings,[80] a report that human female tibial nerves express higher amounts of Sp4 than those from male subjects,[84] suggesting future studies to determine what mechanism(s) underlies these observations.

4.2. Mechanisms for the reversal of pain by mithramycin

The mechanism(s) that underly MTM-dependent reversal of cisplatin (**Fig. 1F**) and oxaliplatin-induced mechanical hypersensitivity (**Figs. 2D and 4C**) remain to be determined.[49,71] Peripheral and central *TRPV1* expression is required for the development and persistence of mechanical hypersensitivity in multiple models of painful hypersensitivity,[19,23,24,29,34,36,93] including cisplatin[92] and oxaliplatin-induced[18] CIPN. Therefore, MTM's ability to block Sp4-dependent *TRPV1* expression may contribute to MTM's reversal of mechanical hypersensitivity. More broadly, Sp4 is coexpressed in a subset of nociceptors

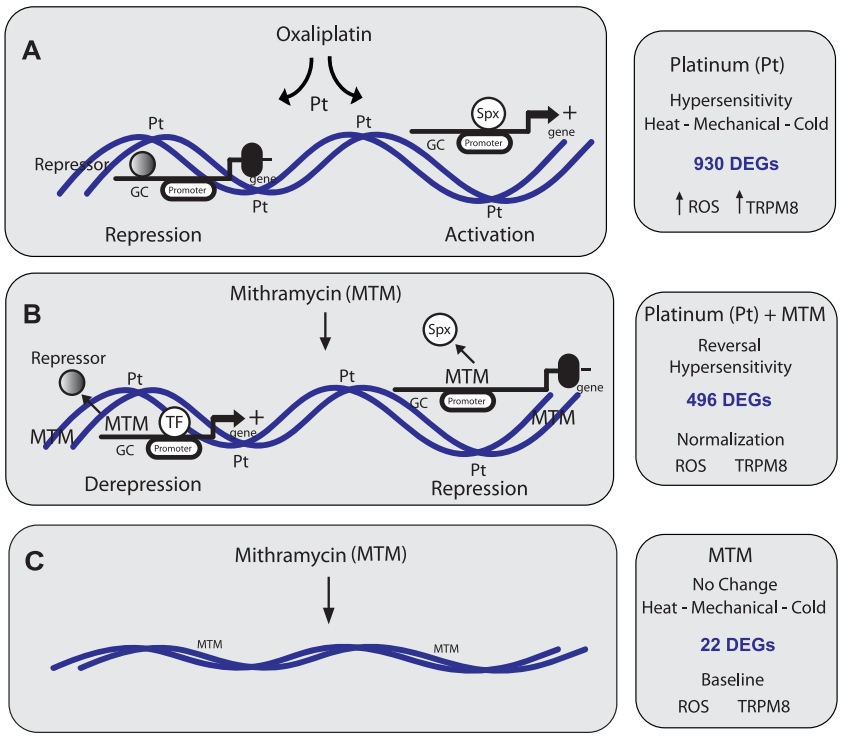

Figure 13. Hypothetical mechanism of mithramycin's (MTM's) reversal of oxaliplatin-induced painful hypersensitivity. (A) Oxaliplatin (platinum - Pt) binds to dorsal root ganglion (DRG) nuclear and mitochondrial DNA forming intrastrand adducts. Oxaliplatin-induced changes in DNA structure allow binding of repressor proteins (left) to genes contributing to antinociception and activation of pronociceptive genes driven by GC box–binding transcription factors Spx such as Sp1 and Sp4. Oxaliplatin-induced transcriptional changes in sensory neurons result in 930 differentially expressed genes (DEGs), a subset of which drive painful hypersensitivity to heat, mechanical and cold stimuli. Oxaliplatin induces an increase in DRG intracellular reactive oxygen species (ROS) known to elicit pain, in part, by activating transient potential (TRP) channels, such as *TRPM8*, shown to mediate cold hypersensitivity. (B) Mithramycin (MTM) binding to GC-rich DNA regulatory domains under conditions of oxaliplatin-induced DNA modification is proposed to reverse oxaliplatin-induced painful hypersensitivity through the inhibition of Spx transcription factor binding and by a combination of derepression of antinociceptive genes such as Mt2 metallothionein and Nts neurotensin (left) and repression of pronociceptive genes such as TRPM8 (right). Changes in 496 DEGs include modulation of genes encoding Complex 1 of the mitochondrial electron transport chain are proposed to contribute to the normalization of ROS levels in oxaliplatin-treated DRG. (C) MTM treatment alone does not significantly bind or alter DRG DNA structure and thus does not change sensory threshold withdrawal values to noxious heat, mechanical or cold stimuli, nor evoke a change in DRG ROS levels or *TRPM8* expression. The small number of MTM-only DEGs (22) likely reflect the limited ability of MTM to access GC-binding domains under conditions without oxaliplatin-induced structural changes.

that bind Isolectin B4 (IB4),[90] with mechanosensitive properties.[6,81] Notably, ablation of IB4+ DRG neurons eliminates oxaliplatin-induced mechanical hypersensitivity.[48] We hypothesize that the ability of MTM to reverse mechanical hypersensitivity induced by cisplatin and oxaliplatin includes its modulation of genes expressed in IB4+, Sp4+ primary afferent neurons. This idea is plausible given that CFA-induced inflammation increases *TRPV1* expression (24% > 80%) in IB4+ DRG neurons,[11] and the majority of IB4+ DRG neurons express Sp4.[90]

Clinically, oxaliplatin is administered in multiple cycles (doses) over time. An increasing cumulative dose leads to greater effectiveness of its anticancer activity, but with increasing risk of neurotoxicity,[12] CIPN, and peripheral neuropathies that include a decrease of intraepidermal nerve fiber (IENF) density in humans[14] and in animal models.[10,103] As shown in **Figs. 4A–C**, persistent cold and mechanical hypersensitivity sustained over 4 weeks of oxaliplatin treatment was reversed following MTM treatment. However, MTM rescue of hypersensitivity observed after 1 month of oxaliplatin did not reverse the oxaliplatin-induced loss of IENF density 7 days after MTM treatment (**Fig. 5**) despite ongoing anatomic evidence of small-fiber neuropathy. This finding supports the hypothesis that loss of IENF is associated with the development of pain behaviors but is not necessary or sufficient for pain persistence.

Which genes underlie MTM's reversal of heat, mechanical, and noxious cold hypersensitivity? To address this question, we applied multiple analytic approaches to DRG RNAseq data derived from oxaliplatin-treated mice with, or without, subsequent MTM rescue. As detailed in **Fig. 7**, MTM treatment alone under control conditions represented the lowest number of DEGs (22) and correlated with stable baseline nociceptive thresholds (**Figs. 1A, 2B–D**). By contrast, MTM rescue of oxaliplatin treatment resulted in 496 DEGs (Supplementary Table 2, available at http://links.lww.com/PAIN/B864). We interpret these findings to suggest that MTM is having its greatest transcriptional impact on DRG gene expression under oxaliplatin-induced neurotoxicity, reflecting de novo access of MTM to Sp1-like regulatory sites. This idea is consistent with our findings showing that MTM-rescue is associated with enrichment of genes regulated by Sp1-like transcription factors (**Figs. 6C, 8C**). We assembled a model of a nociceptor with the functional classification of DEGs identified from MTM rescue that spanned a range of signaling pathways (**Fig. 9**). Then, we applied an unbiased analysis of protein–protein interaction enrichment to identify what genes or gene networks could underly an overarching mechanism of MTM's reversal of painful hypersensitivity.

As shown in **Fig. 10**, the highest scoring interaction identified mitochondrial components of the electron transport chain (ETC).

4.3. Mitochondria and mithramycin

Platinum-based chemotherapy agents like cisplatin and oxaliplatin accumulate and form DNA adducts in DRG that induce DNA/mitochondrial damage, enhancing reactive oxygen species (ROS) production while activating nociceptor-associated channels.[45,63,76,102] Exactly how oxaliplatin or other platinum chemotherapy increase mitochondrial ROS is poorly understood. Nevertheless, increased mitochondrial ROS levels are associated with cisplatin's and oxaliplatin's neurotoxicity in painful CIPN.[50] As a strategy to abrogate platinum-induced elevated mitochondrial ROS, antioxidants were investigated as potential therapeutics. However, no clinically relevant protective effects were found.[54,97] We investigated the role of MTM to reverse oxaliplatin-induced hypersensitivity through mitochondrial ROS.[70] As shown in **Fig. 11**, oxaliplatin-induced increases in ROS in sensory neuronal cultures harvested from mice on day 10 correlated with ongoing cold and mechanical hypersensitivity. By contrast, cotreatment with MTM in vivo not only reversed behavioral hypersensitivity but decreased sensory neuronal ROS levels to baseline on day 10.

Our differential expression and enrichment analyses identified increased expression of 4 (ND1, ND3, ND4, ND4L) of 7 components of the mitochondrial DNA encoded subunits of Complex 1—a major source of ROS production of the ETC.[89] We hypothesize that oxaliplatin-mediated dysfunction of components of complex-1 increase ROS production that is reversed, in part, through MTM-mediated transcriptional regulation of the ETC. This hypothesis is plausible because Complex-1 inhibitors such as rotenone enhance oxaliplatin-induced allodynia[104] and genetic targeting of Complex-1 subunit NDUFA1 produces an increase in ROS.[82,89] Conversely, a point mutation of a component of Complex 1 ND6 (P25L) blocks pathological ROS production.[107]

Certain mitochondrial genes are regulated by nuclear transcription factors,[61] including Sp4, that bigenomically regulates the transcription of all mitochondrial and nuclear encoded genes of cytochrome c oxidase (COX), the terminal enzyme of the ETC.[47] Whether an increase in COX1 or a decrease in Cox4i1 observed following MTM rescue (Supplementary Figure 5, available at http://links.lww.com/PAIN/B865) contributes to the reversal of DRG ROS levels will require further investigation.[7]The ability of MTM to reverse oxaliplatin-induced increases in *TRPM8* expression and its normalization of mitochondrial ROS through modulation of ETC transcription may represent an effective strategy for the relief of painful CIPN as proposed in (**Fig. 13**).[66]

4.4. Limitations and conclusions

Several limitations warrant consideration. Although we provide evidence of MTM's action on the peripheral (nociceptive) system, MTM is known to act on the central nervous system.[32] Therefore, MTM reversal of pain behaviors may involve the regulation of genes and gene networks throughout both the central and peripheral nervous systems. In addition to modulation of mitochondrial ROS production, MTM-directed regulation of alternative splicing of genes enriched for axonal transport represents another potential therapeutic mechanism (**Fig. 12**). Therefore, other genes and gene families may serve to amplify the reversal of painful hypersensitive states. Traumatic nerve injury and CIPN may share common mechanisms such as dependence on Sp1-like factors, which can be blocked by the action of MTM.[37] Although the identification of an FDA-approved anticancer drug with the ability to reverse painful hypersensitivities is clinically appealing, it needs to be approached with caution given its known toxicity.[95] Fortunately, inhibition of Sp1-like transcription does not appear to be a driver for the systemic toxicity reported with the administration of MTM.

The ongoing pain induced by platinum neurotoxicity and observed in patients with CIPN is not fixed, but is being sustained in part, by ongoing neuroplastic changes in pain transduction and mitochondria function that can be reversed through targeted transcriptional therapeutics.

Conflict of interest statement

The authors have no conflict of interest to declare.

Acknowledgements

The work was supported by UCSF Department of Anesthesia and Perioperative Care (M. A. Schumacher), UCSF School of Medicine Springer H. Memorial Foundation (M. A. Schumacher), and National Institutes of Health grant NIH R01CA250017 (J. D. Levine, M. A. Schumacher).

Supplemental digital content

Supplemental digital content associated with this article can be found online at http://links.lww.com/PAIN/B865 and http://links.lww.com/PAIN/B864.

Article history:
Received 20 December 2021
Received in revised form 8 February 2023
Accepted 25 April 2023
Available online 27 June 2023

References

[1] Alloui A, Zimmermann K, Mamet J, Duprat F, Noel J, Chemin J, Guy N, Blondeau N, Voilley N, Rubat-Coudert C, Borsotto M, Romey G, Heurteaux C, Reeh P, Eschalier A, Lazdunski M. TREK-1, a K+ channel involved in polymodal pain perception. EMBO J 2006;25:2368–76.
[2] Amaya F, Oh-hashi K, Naruse Y, Iijima N, Ueda M, Shimosato G, Tominaga M, Tanaka Y, Tanaka M. Local inflammation increases vanilloid receptor 1 expression within distinct subgroups of DRG neurons. Brain Res 2003;963:190–6.
[3] Ang WH, Myint M, Lippard SJ. Transcription inhibition by platinum-DNA cross-links in live mammalian cells. J Am Chem Soc 2010;132:7429–35.
[4] Bader GD, Hogue CW. An automated method for finding molecular complexes in large protein interaction networks. BMC Bioinformatics 2003;4:2.
[5] Bangash MA, Alles SRA, Santana-Varela S, Millet Q, Sikandar S, de Clauser L, Ter Heegde F, Habib AM, Pereira V, Sexton JE, Emery EC, Li S, Luiz AP, Erdos J, Gossage SJ, Zhao J, Cox JJ, Wood JN. Distinct transcriptional responses of mouse sensory neurons in models of human chronic pain conditions. Wellcome Open Res 2018;3:78.
[6] Barabas ME, Kossyreva EA, Stucky CL. TRPA1 is functionally expressed primarily by IB4-binding, non-peptidergic mouse and rat sensory neurons. PLoS One 2012;7:e47988.
[7] Barshad G, Marom S, Cohen T, Mishmar D. Mitochondrial DNA transcription and its regulation: an evolutionary perspective. Trends Genet 2018;34:682–92.
[8] Basbaum AI, Bautista DM, Scherrer G, Julius D. Cellular and molecular mechanisms of pain. Cell 2009;139:267–84.
[9] Bautista DM, Siemens J, Glazer JM, Tsuruda PR, Basbaum AI, Stucky CL, Jordt SE, Julius D. The menthol receptor TRPM8 is the principal detector of environmental cold. Nature 2007;448:204–8.

[10] Boyette-Davis J, Xin W, Zhang H, Dougherty PM. Intraepidermal nerve fiber loss corresponds to the development of taxol-induced hyperalgesia and can be prevented by treatment with minocycline. PAIN 2011;152:308–13.
[11] Breese NM, George AC, Pauers LE, Stucky CL. Peripheral inflammation selectively increases TRPV1 function in IB4-positive sensory neurons from adult mouse. PAIN 2005;115:37–49.
[12] Brouwers EE, Huitema AD, Beijnen JH, Schellens JH. Long-term platinum retention after treatment with cisplatin and oxaliplatin. BMC Clin Pharmacol 2008;8:7.
[13] Brown JH, Kennedy BJ. Mithramycin in the treatment of disseminated testicular neoplasms. N Engl J Med 1965;272:111–8.
[14] Burakgazi AZ, Messersmith W, Vaidya D, Hauer P, Hoke A, Polydefkis M. Longitudinal assessment of oxaliplatin-induced neuropathy. Neurology 2011;77:980–6.
[15] Caterina MJ, Leffler A, Malmberg AB, Martin WJ, Trafton J, Petersen-Zeitz KR, Koltzenburg M, Basbaum AI, Julius D. Impaired nociception and pain sensation in mice lacking the capsaicin receptor. Science 2000;288:306–13.
[16] Caterina MJ, Schumacher MA, Tominaga M, Rosen TA, Levine JD, Julius D. The capsaicin receptor: a heat-activated ion channel in the pain pathway. Nature 1997;389:816–24.
[17] Chaplan SR, Bach FW, Pogrel JW, Chung JM, Yaksh TL. Quantitative assessment of tactile allodynia in the rat paw. J Neurosci Methods 1994;53:55–63.
[18] Chen K, Zhang ZF, Liao MF, Yao WL, Wang J, Wang XR. Blocking PAR2 attenuates oxaliplatin-induced neuropathic pain via TRPV1 and releases of substance P and CGRP in superficial dorsal horn of spinal cord. J Neurol Sci 2015;352:62–7.
[19] Christoph T, Gillen C, Mika J, Grunweller A, Schafer MK, Schiene K, Frank R, Jostock R, Bahrenberg G, Weihe E, Erdmann VA, Kurreck J. Antinociceptive effect of antisense oligonucleotides against the vanilloid receptor VR1/TRPV1. Neurochem Int 2007;50:281–90.
[20] Chu C, Zavala K, Fahimi A, Lee J, Xue Q, Eilers H, Schumacher MA. Transcription factors Sp1 and Sp4 regulate TRPV1 gene expression in rat sensory neurons. Mol Pain 2011;7:44.
[21] Collin R, Griffiths H, Polacarz SV, Lawrence AC, Watmore A. Mithramycin therapy for resistant hypercalcaemia in transformed chronic granulocytic leukaemia. Clin Lab Haematol 1989;11:156–9.
[22] Conesa A, Madrigal P, Tarazona S, Gomez-Cabrero D, Cervera A, McPherson A, Szczesniak MW, Gaffney DJ, Elo LL, Zhang X, Mortazavi A. A survey of best practices for RNA-seq data analysis. Genome Biol 2016;17:13.
[23] Cui M, Honore P, Zhong C, Gauvin D, Mikusa J, Hernandez G, Chandran P, Gomtsyan A, Brown B, Bayburt EK, Marsh K, Bianchi B, McDonald H, Niforatos W, Neelands TR, Moreland RB, Decker MW, Lee CH, Sullivan JP, Faltynek CR. TRPV1 receptors in the CNS play a key role in broad-spectrum analgesia of TRPV1\ antagonists. J Neurosci 2006;26:9385–93.
[24] Cui YY, Xu H, Wu HH, Qi J, Shi J, Li YQ. Spatio-temporal expression and functional involvement of transient receptor potential vanilloid 1 in diabetic mechanical allodynia in rats. PLoS One 2014;9:e102052.
[25] Davies J, Trask C, Souhami RL. Effect of mithramycin on widespread painful bone metastases in cancer of the breast. Cancer Treat Rep 1979;63:1835–8.
[26] Davis JB, Gray J, Gunthorpe MJ, Hatcher JP, Davey PT, Overend P, Harries MH, Latcham J, Clapham C, Atkinson K, Hughes SA, Rance K, Grau E, Harper AJ, Pugh PL, Rogers DC, Bingham S, Randall A, Sheardown SA. Vanilloid receptor-1 is essential for inflammatory thermal hyperalgesia. Nature 2000;405:183–7.
[27] Descoeur J, Pereira V, Pizzoccaro A, Francois A, Ling B, Maffre V, Couette B, Busserolles J, Courteix C, Noel J, Lazdunski M, Eschalier A, Authier N, Bourinet E. Oxaliplatin-induced cold hypersensitivity is due to remodelling of ion channel expression in nociceptors. EMBO Mol Med 2011;3:266–78.
[28] Diogenes A, Akopian AN, Hargreaves KM. NGF up-regulates TRPA1: implications for orofacial pain. J Dent Res 2007;86:550–5.
[29] Eskander MA, Ruparel S, Green DP, Chen PB, Por ED, Jeske NA, Gao X, Flores ER, Hargreaves KM. Persistent nociception triggered by nerve growth factor (NGF) is mediated by TRPV1 and oxidative mechanisms. J Neurosci 2015;35:8593–603.
[30] Ewels P, Magnusson M, Lundin S, Kaller M. MultiQC: summarize analysis results for multiple tools and samples in a single report. Bioinformatics 2016;32:3047–8.
[31] Fernandez-Guizan A, Mansilla S, Barcelo F, Vizcaino C, Nunez LE, Moris F, Gonzalez S, Portugal J. The activity of a novel mithramycin analog is related to its binding to DNA, cellular accumulation, and inhibition of Sp1-driven gene transcription. Chem Biol Interact 2014;219:123–32.
[32] Ferrante RJ, Ryu H, Kubilus JK, D'Mello S, Sugars KL, Lee J, Lu P, Smith K, Browne S, Beal MF, Kristal BS, Stavrovskaya IG, Hewett S, Rubinsztein DC, Langley B, Ratan RR. Chemotherapy for the brain: the antitumor antibiotic mithramycin prolongs survival in a mouse model of Huntington's disease. J Neurosci 2004;24:10335–42.
[33] Fields AT, Lee MC, Mayer F, Santos YA, Bainton CMV, Matthay ZA, Callcut RA, Mayer N, Cuschieri J, Kober KM, Bainton RJ, Kornblith LZ. A new trauma frontier: exploratory pilot study of platelet transcriptomics in trauma patients. J Trauma Acute Care Surg 2022;92:313–22.
[34] Flynn R, Chapman K, Iftinca M, Aboushousha R, Varela D, Altier C. Targeting the transient receptor potential vanilloid type 1 (TRPV1) assembly domain attenuates inflammation-induced hypersensitivity. J Biol Chem 2014;289:16675–87.
[35] Gauchan P, Andoh T, Kato A, Kuraishi Y. Involvement of increased expression of transient receptor potential melastatin 8 in oxaliplatin-induced cold allodynia in mice. Neurosci Lett 2009;458:93–5.
[36] Gavva NR, Tamir R, Qu Y, Klionsky L, Zhang TJ, Immke D, Wang J, Zhu D, Vanderah TW, Porreca F, Doherty EM, Norman MH, Wild KD, Bannon AW, Louis JC, Treanor JJ. AMG 9810 [(E)-3-(4-t-butylphenyl)-N-(2,3-dihydrobenzo[b][1,4] dioxin-6-yl)acrylamide], a novel vanilloid receptor 1 (TRPV1) antagonist with antihyperalgesic properties. J Pharmacol Exp Ther 2005;313:474–84.
[37] Gomez K, Sandoval A, Barragan-Iglesias P, Granados-Soto V, Delgado-Lezama R, Felix R, Gonzalez-Ramirez R. Transcription factor Sp1 regulates the expression of calcium channel alpha2delta-1 subunit in neuropathic pain. Neuroscience 2019;412:207–15.
[38] Gregg RW, Molepo JM, Monpetit VJ, Mikael NZ, Redmond D, Gadia M, Stewart DJ. Cisplatin neurotoxicity: the relationship between dosage, time, and platinum concentration in neurologic tissues, and morphologic evidence of toxicity. J Clin Oncol 1992;10:795–803.
[39] Gregus AM, Doolen S, Dumlao DS, Buczynski MW, Takasusuki T, Fitzsimmons BL, Hua XY, Taylor BK, Dennis EA, Yaksh TL. Spinal 12-lipoxygenase-derived hepoxilin A3 contributes to inflammatory hyperalgesia via activation of TRPV1 and TRPA1 receptors. Proc Natl Acad Sci U S A 2012;109:6721–6.
[40] Grohar PJ, Woldemichael GM, Griffin LB, Mendoza A, Chen QR, Yeung C, Currier DG, Davis S, Khanna C, Khan J, McMahon JB, Helman LJ. Identification of an inhibitor of the EWS-FLI1 oncogenic transcription factor by high-throughput screening. J Natl Cancer Inst 2011;103:962–78.
[41] Guan Z, Hellman J, Schumacher M. Contemporary views on inflammatory pain mechanisms: TRPing over innate and microglial pathways. F1000Res 2016;5:F1000 Faculty Rev-2425.
[42] Hargreaves K, Dubner R, Brown F, Flores C, Joris J. A new and sensitive method for measuring thermal nociception in cutaneous hyperalgesia. PAIN 1988;32:77–88.
[43] Heath DA. The role of mithramycin in the management of Paget's disease. Metab Bone Dis Relat Res 1981;3:343–5.
[44] Hochberg Y, Benjamini Y. More powerful procedures for multiple significance testing. Stat Med 1990;9:811–8.
[45] Hu X, Jiang Z, Teng L, Yang H, Hong D, Zheng D, Zhao Q. Platinum-induced peripheral neuropathy (PIPN): ROS-related mechanism, therapeutic agents, and nanosystems. Front Mol Biosci 2021;8:770808.
[46] Jacobs SS, Fox E, Dennie C, Morgan LB, McCully CL, Balis FM. Plasma and cerebrospinal fluid pharmacokinetics of intravenous oxaliplatin, cisplatin, and carboplatin in nonhuman primates. Clin Cancer Res 2005;11:1669–74.
[47] Johar K, Priya A, Dhar S, Liu Q, Wong-Riley MT. Neuron-specific specificity protein 4 bigenomically regulates the transcription of all mitochondria- and nucleus-encoded cytochrome c oxidase subunit genes in neurons. J Neurochem 2013;127:496–508.
[48] Joseph EK, Chen X, Bogen O, Levine JD. Oxaliplatin acts on IB4-positive nociceptors to induce an oxidative stress-dependent acute painful peripheral neuropathy. J Pain 2008;9:463–72.
[49] Joseph EK, Levine JD. Comparison of oxaliplatin- and cisplatin-induced painful peripheral neuropathy in the rat. J Pain 2009;10:534–41.
[50] Kelley MR, Jiang Y, Guo C, Reed A, Meng H, Vasko MR. Role of the DNA base excision repair protein, APE1 in cisplatin, oxaliplatin, or carboplatin induced sensory neuropathy. PLoS One 2014;9:e106485.
[51] Knowlton WM, Bifolck-Fisher A, Bautista DM, McKemy DD. TRPM8, but not TRPA1, is required for neural and behavioral responses to acute noxious cold temperatures and cold-mimetics in vivo. PAIN 2010;150:340–50.
[52] Kober KM, Schumacher M, Conley YP, Topp K, Mazor M, Hammer MJ, Paul SM, Levine JD, Miaskowski C. Signaling pathways and gene co-expression modules associated with cytoskeleton and axon

morphology in breast cancer survivors with chronic paclitaxel-induced peripheral neuropathy. Mol Pain 2019;15:1744806919878088.
[53] Koscielny G, An P, Carvalho-Silva D, Cham JA, Fumis L, Gasparyan R, Hasan S, Karamanis N, Maguire M, Papa E, Pierleoni A, Pignatelli M, Platt T, Rowland F, Wankar P, Bento AP, Burdett T, Fabregat A, Forbes S, Gaulton A, Gonzalez CY, Hermjakob H, Hersey A, Jupe S, Kafkas S, Keays M, Leroy C, Lopez FJ, Magarinos MP, Malone J, McEntyre J, Munoz-Pomer Fuentes A, O'Donovan C, Papatheodorou I, Parkinson H, Palka B, Paschall J, Petryszak R, Pratanwanich N, Sarntivijal S, Saunders G, Sidiropoulos K, Smith T, Sondka Z, Stegle O, Tang YA, Turner E, Vaughan B, Vrousgou O, Watkins X, Martin MJ, Sanseau P, Vamathevan J, Birney E, Barrett J, Dunham I. Open targets: a platform for therapeutic target identification and validation. Nucleic Acids Res 2017;45:D985–94.
[54] Kottschade LA, Sloan JA, Mazurczak MA, Johnson DB, Murphy BP, Rowland KM, Smith DA, Berg AR, Stella PJ, Loprinzi CL. The use of vitamin E for the prevention of chemotherapy-induced peripheral neuropathy: results of a randomized phase III clinical trial. Support Care Cancer 2011;19:1769–77.
[55] Kroigard T, Schroder HD, Qvortrup C, Eckhoff L, Pfeiffer P, Gaist D, Sindrup SH. Characterization and diagnostic evaluation of chronic polyneuropathies induced by oxaliplatin and docetaxel comparing skin biopsy to quantitative sensory testing and nerve conduction studies. Eur J Neurol 2014;21:623–9.
[56] Kukurba KR, Montgomery SB. RNA sequencing and analysis. Cold Spring Harb Protoc 2015;2015:951–69.
[57] Kushnareva Y, Murphy AN, Andreyev A. Complex I-mediated reactive oxygen species generation: modulation by cytochrome c and NAD(P)+ oxidation-reduction state. Biochem J 2002;368:545–53.
[58] Lacroix-Fralish ML, Ledoux JB, Mogil JS. The pain genes database: an interactive web browser of pain-related transgenic knockout studies. PAIN 2007;131:3 e1–4.
[59] Landau WM, Liu P. Dispersion estimation and its effect on test performance in RNA-seq data analysis: a simulation-based comparison of methods. PLoS One 2013;8:e81415.
[60] Leek JT, Storey JD. Capturing heterogeneity in gene expression studies by surrogate variable analysis. PLoS Genet 2007;3:1724–35.
[61] Leigh-Brown S, Enriquez JA, Odom DT. Nuclear transcription factors in mammalian mitochondria. Genome Biol 2010;11:215.
[62] Lennertz RC, Kossyreva EA, Smith AK, Stucky CL. TRPA1 mediates mechanical sensitization in nociceptors during inflammation. PLoS One 2012;7:e43597.
[63] Leo M, Schmitt LI, Kusterarent P, Kutritz A, Rassaf T, Kleinschnitz C, Hendgen-Cotta UB, Hagenacker T. Platinum-based drugs cause mitochondrial dysfunction in cultured dorsal root ganglion neurons. Int J Mol Sci 2020;21:8636.
[64] Liao Y, Smyth GK, Shi W. featureCounts: an efficient general purpose program for assigning sequence reads to genomic features. Bioinformatics 2014;30:923–30.
[65] Lombo F, Menendez N, Salas JA, Mendez C. The aureolic acid family of antitumor compounds: structure, mode of action, biosynthesis, and novel derivatives. Appl Microbiol Biotechnol 2006;73:1–14.
[66] Ma J, Kavelaars A, Dougherty PM, Heijnen CJ. Beyond symptomatic relief for chemotherapy-induced peripheral neuropathy: targeting the source. Cancer 2018;124:2289–98.
[67] MacDonald DI, Luiz AP, Iseppon F, Millet Q, Emery EC, Wood JN. Silent cold-sensing neurons contribute to cold allodynia in neuropathic pain. Brain 2021;144:1711–26.
[68] MacDonald DI, Wood JN, Emery EC. Molecular mechanisms of cold pain. Neurobiol Pain 2020;7:100044.
[69] Maglott D, Ostell J, Pruitt KD, Tatusova T. Entrez gene: gene-centered information at NCBI. Nucleic Acids Res 2011;39:D52–7.
[70] Makarevich O, Sabirzhanov B, Aubrecht TG, Glaser EP, Polster BM, Henry RJ, Faden AI, Stoica BA. Mithramycin selectively attenuates DNA-damage-induced neuronal cell death. Cell Death Dis 2020;11:587.
[71] McDonald ES, Randon KR, Knight A, Windebank AJ. Cisplatin preferentially binds to DNA in dorsal root ganglion neurons in vitro and in vivo: a potential mechanism for neurotoxicity. Neurobiol Dis 2005;18:305–13.
[72] McKemy DD, Neuhausser WM, Julius D. Identification of a cold receptor reveals a general role for TRP channels in thermosensation. Nature 2002;416:52–8.
[73] Meloto CB, Benavides R, Lichtenwalter RN, Wen X, Tugarinov N, Zorina-Lichtenwalter K, Chabot-Dore AJ, Piltonen MH, Cattaneo S, Verma V, Klares R III, Khoury S, Parisien M, Diatchenko L. Human pain genetics database: a resource dedicated to human pain genetics research. PAIN 2018;159:749–63.
[74] Miaskowski C, Mastick J, Paul SM, Topp K, Smoot B, Abrams G, Chen LM, Kober KM, Conley YP, Chesney M, Bolla K, Mausisa G, Mazor M, Wong M, Schumacher M, Levine JD. Chemotherapy-induced neuropathy in cancer survivors. J Pain Symptom Manage 2017;54:204–18.e2.
[75] Miltenburg NC, Boogerd W. Chemotherapy-induced neuropathy: a comprehensive survey. Cancer Treat Rev 2014;40:872–82.
[76] Miyake T, Nakamura S, Zhao M, So K, Inoue K, Numata T, Takahashi N, Shirakawa H, Mori Y, Nakagawa T, Kaneko S. Cold sensitivity of TRPA1 is unveiled by the prolyl hydroxylation blockade-induced sensitization to ROS. Nat Commun 2016;7:12840.
[77] Morin C, Bushnell CM. Temporal and qualitative properties of cold pain and heat pain: a psychophysical study. PAIN 1998;74:67–73.
[78] Okun A, DeFelice M, Eyde N, Ren J, Mercado R, King T, Porreca F. Transient inflammation-induced ongoing pain is driven by TRPV1 sensitive afferents. Mol Pain 2011;7:4.
[79] Pachman DR, Loprinzi CL, Grothey A, Ta LE. The search for treatments to reduce chemotherapy-induced peripheral neuropathy. J Clin Invest 2014;124:72–4.
[80] Patil MJ, Ruparel SB, Henry MA, Akopian AN. Prolactin regulates TRPV1, TRPA1, and TRPM8 in sensory neurons in a sex-dependent manner: contribution of prolactin receptor to inflammatory pain. Am J Physiol Endocrinol Metab 2013;305:E1154–64.
[81] Pinto LG, Souza GR, Kusuda R, Lopes AH, Sant'Anna MB, Cunha FQ, Ferreira SH, Cunha TM. Non-Peptidergic nociceptive neurons are essential for mechanical inflammatory hypersensitivity in mice. Mol Neurobiol 2019;56:5715–28.
[82] Qi X, Lewin AS, Hauswirth WW, Guy J. Suppression of complex I gene expression induces optic neuropathy. Ann Neurol 2003;53:198–205.
[83] Quarni W, Dutta R, Green R, Katiri S, Patel B, Mohapatra SS, Mohapatra S. Mithramycin A inhibits colorectal cancer growth by targeting cancer stem cells. Sci Rep 2019;9:15202.
[84] Ray PR, Khan J, Wangzhou A, Tavares-Ferreira D, Akopian AN, Dussor G, Price TJ. Transcriptome analysis of the human tibial nerve identifies sexually dimorphic expression of genes involved in pain, inflammation, and neuro-immunity. Front Mol Neurosci 2019;12:37.
[85] Reichling DB, Levine JD. Heat transduction in rat sensory neurons by calcium-dependent activation of a cation channel. Proc Natl Acad Sci U S A 1997;94:7006–11.
[86] Ren K, Dubner R. Inflammatory models of pain and hyperalgesia. ILAR J 1999;40:111–8.
[87] Robinson MD, McCarthy DJ, Smyth GK. edgeR: a Bioconductor package for differential expression analysis of digital gene expression data. Bioinformatics 2010;26:139–40.
[88] Schmittgen TD, Livak KJ. Analyzing real-time PCR data by the comparative C(T) method. Nat Protoc 2008;3:1101–8.
[89] Sharma LK, Lu J, Bai Y. Mitochondrial respiratory complex I: structure, function and implication in human diseases. Curr Med Chem 2009;16:1266–77.
[90] Sheehan K, Lee J, Chong J, Zavala K, Sharma M, Philipsen S, Maruyama T, Xu Z, Guan Z, Eilers H, Kawamata T, Schumacher M. Transcription factor Sp4 is required for hyperalgesic state persistence. PLoS One 2019;14:e0211349.
[91] Shen S, Park JW, Lu ZX, Lin L, Henry MD, Wu YN, Zhou Q, Xing Y. rMATS: robust and flexible detection of differential alternative splicing from replicate RNA-Seq data. Proc Natl Acad Sci U S A 2014;111:E5593–601.
[92] Shim HS, Bae C, Wang J, Lee KH, Hankerd KM, Kim HK, Chung JM, La JH. Peripheral and central oxidative stress in chemotherapy-induced neuropathic pain. Mol pain 2019;15:1744806919840098.
[93] Shinoda M, Ogino A, Ozaki N, Urano H, Hironaka K, Yasui M, Sugiura Y. Involvement of TRPV1 in nociceptive behavior in a rat model of cancer pain. J Pain 2008;9:687–99.
[94] Sisignano M, Baron R, Scholich K, Geisslinger G. Mechanism-based treatment for chemotherapy-induced peripheral neuropathic pain. Nat Rev Neurol 2014;10:694–707.
[95] Sissung TM, Huang PA, Hauke RJ, McCrea EM, Peer CJ, Barbier RH, Strope JD, Ley AM, Zhang M, Hong JA, Venzon D, Jackson JP, Brouwer KR, Grohar P, Glod J, Widemann BC, Heller T, Schrump DS, Figg WD. Severe hepatotoxicity of mithramycin therapy caused by altered expression of hepatocellular bile transporters. Mol Pharmacol 2019;96:158–67.
[96] Snyder RC, Ray R, Blume S, Miller DM. Mithramycin blocks transcriptional initiation of the c-myc P1 and P2 promoters. Biochemistry 1991;30:4290–7.
[97] Stankovic JSK, Selakovic D, Mihailovic V, Rosic G. Antioxidant supplementation in the treatment of neurotoxicity induced by

platinum-based chemotherapeutics—a review. Int J Mol Sci 2020;21:7753.
[98] Starobova H, Mueller A, Deuis JR, Carter DA, Vetter I. Inflammatory and neuropathic gene expression signatures of chemotherapy-induced neuropathy induced by vincristine, cisplatin, and oxaliplatin in C57BL/6J mice. J Pain 2020;21:182–94.
[99] Ta LE, Bieber AJ, Carlton SM, Loprinzi CL, Low PA, Windebank AJ. Transient Receptor Potential Vanilloid 1 is essential for cisplatin-induced heat hyperalgesia in mice. Mol pain 2010;6:15.
[100] Thul PJ, Lindskog C. The human protein atlas: a spatial map of the human proteome. Protein Sci 2018;27:233–44.
[101] Ule J, Blencowe BJ. Alternative splicing regulatory networks: functions, mechanisms, and evolution. Mol Cell 2019;76:329–45.
[102] van Hameren G, Campbell G, Deck M, Berthelot J, Gautier B, Quintana P, Chrast R, Tricaud N. In vivo real-time dynamics of ATP and ROS production in axonal mitochondria show decoupling in mouse models of peripheral neuropathies. Acta Neuropathol Commun 2019;7:86.
[103] Warncke UO, Toma W, Meade JA, Park AJ, Thompson DC, Caillaud M, Bigbee JW, Bryant CD, Damaj MI. Impact of dose, sex, and strain on oxaliplatin-induced peripheral neuropathy in mice. Front Pain Res (Lausanne) 2021;2:683168.
[104] Xiao WH, Bennett GJ. Effects of mitochondrial poisons on the neuropathic pain produced by the chemotherapeutic agents, paclitaxel and oxaliplatin. Pain 2012;153:704–9.
[105] Xue Q, Jong B, Chen T, Schumacher MA. Transcription of rat TRPV1 utilizes a dual promoter system that is positively regulated by nerve growth factor. J Neurochem 2007;101:212–22.
[106] Yang C, Zhou Q, Li M, Tong X, Sun J, Qing Y, Sun L, Yang X, Hu X, Jiang J, Yan X, He L, Wan C. Upregulation of CYP2S1 by oxaliplatin is associated with p53 status in colorectal cancer cell lines. Sci Rep 2016;6:33078.
[107] Yin Z, Burger N, Kula-Alwar D, Aksentijevic D, Bridges HR, Prag HA, Grba DN, Viscomi C, James AM, Mottahedin A, Krieg T, Murphy MP, Hirst J. Structural basis for a complex I mutation that blocks pathological ROS production. Nat Commun 2021;12:707.
[108] Zavala K, Lee J, Chong J, Sharma M, Eilers H, Schumacher MA. The anticancer antibiotic mithramycin-A inhibits TRPV1 expression in dorsal root ganglion neurons. Neurosci Lett 2014;578:211–6.
[109] Zerbino DR, Achuthan P, Akanni W, Amode MR, Barrell D, Bhai J, Billis K, Cummins C, Gall A, Giron CG, Gil L, Gordon L, Haggerty L, Haskell E, Hourlier T, Izuogu OG, Janacek SH, Juettemann T, To JK, Laird MR, Lavidas I, Liu Z, Loveland JE, Maurel T, McLaren W, Moore B, Mudge J, Murphy DN, Newman V, Nuhn M, Ogeh D, Ong CK, Parker A, Patricio M, Riat HS, Schuilenburg H, Sheppard D, Sparrow H, Taylor K, Thormann A, Vullo A, Walts B, Zadissa A, Frankish A, Hunt SE, Kostadima M, Langridge N, Martin FJ, Muffato M, Perry E, Ruffier M, Staines DM, Trevanion SJ, Aken BL, Cunningham F, Yates A, Flicek P. Ensembl 2018. Nucleic Acids Res 2018;46:D754–61.
[110] Zhao JY, Liang L, Gu X, Li Z, Wu S, Sun L, Atianjoh FE, Feng J, Mo K, Jia S, Lutz BM, Bekker A, Nestler EJ, Tao YX. DNA methyltransferase DNMT3a contributes to neuropathic pain by repressing Kcna2 in primary afferent neurons. Nat Commun 2017;8:14712.
[111] Zhu J, Vinothkumar KR, Hirst J. Structure of mammalian respiratory complex I. Nature 2016;536:354–8.